5-1-2010

EFFECTS OF INTERNAL FIELDS IN QUANTUM DOTS

Sasi Sekaran Sundaresan
Southern Illinois University Carbondale, sasi@siu.edu

Recommended Citation

Sundaresan, Sasi Sekaran, "EFFECTS OF INTERNAL FIELDS IN QUANTUM DOTS" (2010). *Theses.* Paper 244.

EFFECTS OF INTERNAL FIELDS IN QUANTUM DOTS

by

Sasi Sekaran Sundaresan

B.E., Anna University, 2008

A Thesis
Submitted in Partial Fulfillment of the Requirements for the
Master of Science Degree

Department of Electrical and Computer Engineering
In the Graduate School
Southern Illinois University Carbondale
May 2010

THESIS APPROVAL

EFFECTS OF INTERNAL FIELDS IN QUANTUM DOTS

By

Sasi Sekaran Sundaresan

A Thesis Submitted in Partial

Fulfillment of the Requirements

For the Degree of

Master of Science

in the field of Electrical and Computer Engineering

Approved by:

Dr. Shaikh Ahmed, Chair

Dr. Haibo Wang

Dr. Mohammed Sayeh

Graduate School
Southern Illinois University Carbondale
April 6th, 2010

AN ABSTRACT OF THE THESIS OF

SASI SEKARAN SUNDARESAN, for the Master of Science degree in Electrical and Computer Engineering, presented on April 6th 2010, at Southern Illinois University Carbondale.

TITLE: EFFECTS OF INTERNAL FIELDS IN QUANTUM DOTS

MAJOR PROFESSOR: Dr. Shaikh S Ahmed

In this work we study the effect of built in electrostatic fields in Quantum Dots. Built-in electrostatic fields in Zincblende quantum dots originate mainly from—(1) the fundamental crystal atomicity and the interfaces between two dissimilar materials, (2) the strain relaxation, and (3) the piezoelectric polarization. We also study the geometric dependence of built in fields on 3 shapes namely Box, Dome and Pyramid. The main objectives are 3 fold they are (1) Explore the nature and the role of crystal atomicity at the interfaces and built-in fields (strain-field, and piezoelectric polarization) in determining the energy spectrum and the wave functions. (2) To identify the shift in the one-particle energy states, symmetry-lowering and non-degeneracy in the first excited state and strong band-mixing in the overall conduction band electronic states. (3) Finally geometric dependence of the above-mentioned phenomena. We discuss the importance atomistic effects and the need for 3 dimensional atomistic simulator NEMO 3D. We also discuss the effect of built in fields in HEMT (High Electron Mobility Transistor).

ACKNOWLEDGMENTS

I would like to formally thank Dr. Shaikh S Ahmed for all of his advice and support throughout this thesis project. I would also like to give my hearty thanks to my family and friends for their support as I could not have done it without them.

TABLE OF CONTENTS

LIST OF TABLES

LIST OF FIGURES

CHAPTER 1

INTRODUCTION

The semiconductor industry has been the largest industry with a global market of $260 billion in 2009, the industry enables the generation of some $1,200 billion in electronic systems and $5,000 billion in services, representing close to 10% of world GDP. The revolution of semiconductor industry was sparked by the invention of transistors in 1948 at Bell Telephone Laboratories. The transistors replaced the thermionic valve, which was invented by John Fleming in 1904. Later the development of reliable high quality oxide growth over silicon layer and the demonstration of the planar process, with Silicon dioxide (SiO2) layer acting as excellent barrier for selective diffusion steps, led to the invention of silicon based bipolar integrated circuits (ICs) in 1959[1]. Addition of silicon gate process, with low interface-state density of the Si/SiO2 materials gave rise to Field Effect Devices (e.g. Field Effect Transistor). In 1968, Metal Oxide Field Effect Transistor (MOSFET) was discovered. The discovery of MOSFET was the most important foundation for today's semiconductor industry. Their performance has enabled power consumptions in ICs to be reduced. The hunger of device down scaling led to the evolution of Nano-scale devices. Carbon Nano Tubes (CNT), were most promising devices exhibiting good material and electrical properties. These innovations resulted in a significant reduction in power dissipation and overlap capacitance. The search for devices having properties that are between those of bulk semiconductors and those of discrete molecules led to the invention of Quantum dots.

1.1 DEVICE SCALING

Over the past decade, the semiconductor devices have continually been scaled down in size. The MOSFET channel lengths were once several micrometers, but modern integrated circuits are incorporating MOSFETs with channel lengths of less than 32 nanometers. The semiconductor industry maintains a "roadmap", the ITRS, which sets the pace for development of innovative technology [3].

Moore's law states doubling of transistor performance and quadrupling of the number of devices on a chip every 3 years. The phenomenal progress signified by Moore's law has been achieved through scaling down the MOSFET size[1]. The scaling of CMOS technology has progressed relentlessly from 10 um in 1970's to present day line width of 32 nm.

Fig. 1.1 shows a current trend in technology evolution [13]. The below figure shows the change in gate length (*L_gate*), drain voltage (V_{dd}), gate oxide thickness (T_{OX}) and threshold voltage (V_{th}). We can see that operating drain voltage (V_{dd}), threshold voltage (V_{th}), and, to a lesser extent, gate oxide thickness (T_{OX}) has decreased more slowly than *L_gate*, while I_D_sat (NMOS device) has remained more or less fixed [13].

CMOS Technology Roadmap
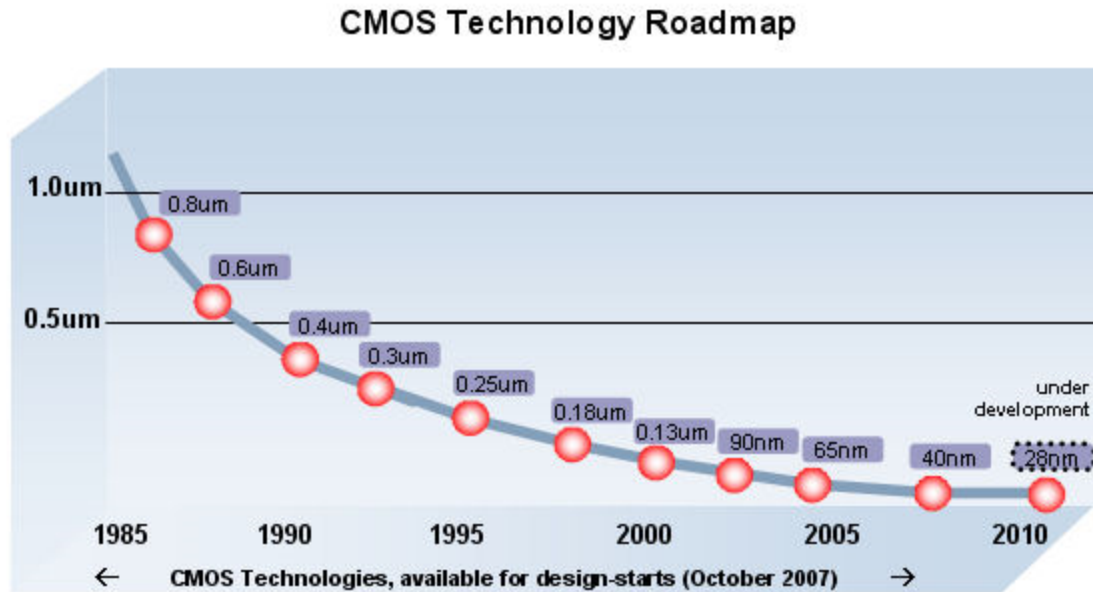
Figure 1.1 CMOS Technology Roadmap for Integrated Circuits, from Ref [4]

There are 3 major things that characterize the improvement of semiconductor industry in this era, they are (1) Extreme devotion to scaling by continued and constant improvements in lithography. (2) An average amount of effort in modifying the architecture, e.g. introduction of SOI devices, FINFETS, GFETs, Quantum Dots etc. (3) A minimal introduction of new materials with lesser band gap (E_g), e.g. Si has a E_g = 1.12 eV and Ge has E_g = 0.69 eV, when Si is replaced with Ge threshold voltage (V_t) decreases hence the applied Gate voltage (V_g) decreases in the case of FETs.

Semiconductors derive their great importance from the fact that their electrical conductivity can be greatly altered via an external stimulus (voltage, photon flux, etc), making semiconductors critical parts of many different kinds of electrical circuits and optical applications. Quantum dots are unique class of

semiconductor because they are so small, ranging from 2-10 nanometers (10-50 atoms) in diameter. At these small sizes materials behave differently, giving quantum dots unprecedented tuning ability and enabling never before seen applications to science and technology. It is possible to have very precise control over the conductive properties of the material.

1.2 NEED FOR NEW DEVICES

The fundamental limits on device scaling has led to pessimistic predictions of the imminent end of technological progress for the semiconductor industry and simultaneously have increased interest in advanced alternative technologies. It is suggested that the current rate of transistor performance improvement i.e. in accordance with Moore's Law, can only sustain for another 10 to 15 years, but only through the development and introduction of new materials and structures. In addition, an enormous improvement in lithographic techniques will be required to continue device scaling. Expectations run high that these novel technologies.

In order to achieve the above aspects we focus on two methods they are: *new materials* and *new device structures*. The introduction of a new material (like GaN substrate, AlGaN channel) requires the use of a new device structure (Quantum Dots, heterojunction transistors, SOI etc), or vice versa.

Emergence of Quantum mechanics marked birth of new class of devices, where the wave nature of electron was emphasized. The reduction in size to <10 nm in these devices has led to pronounced Quantum mechanical effects in these devices. Hence it is necessary to engineer these quantum mechanical effects to

increase the device performances; the Quantum Dot is one such example. Quantum Dots (QD) form basis for new set of optoelectronic devices. Quantum dots offer application opportunities in optical sensors, lasers, and advanced electronic devices for memory and logic. Technology developer "*InVisage Technologies*" has announced sensors it says can offer four times better performance than conventional CCD and CMOS sensors. The company's 'QuantumFilm' technology uses the unique electronic behavior of quantum dots (precisely-sized nano-scale crystals trapped in a polymer film) to replace conventional silicon photodiodes. The company says the quantum dots themselves are twice as sensitive to light as conventional photodiodes

Another example is High Electron Mobility Transistors (HEMT). The concept of a band-engineered transistor is to enhance the mobility of electrons and/or holes in the channel by modifying the band structure of silicon in the channel in a way such that the physical structure of the transistor remains substantially unchanged. HEMT's make use of variations in energy band gap besides electric field to control the forces acting on electrons and holes separately and independently of each other [12]. The resulting greater design freedom permits the emergence of high speed devices. This enhanced mobility increases the transistor transconductance (g_m) and on-drive current (I_{on}). An AlGaN layer or a GaN layer is used as the enhanced-mobility channel layer. These Heterostructure FET or High Electron Mobility Transistors (HEMT) has seen a massive increase in research effort, due to their high-power performance.

1.3 QUANTUM DOTS:

Quantum Dots are man-made artificial atoms that confine electrons to a small space. A quantum dot is a semiconductor whose excitons (electron-hole pairs) or in other words charges are confined in all three spatial dimensions. As a result, they have properties that are between those of bulk semiconductors and those of discrete molecules. They were discovered by Louis E. Brus in the year 1983, who was then at Bell Labs. The term "Quantum Dot" was coined by Mark Reed. Quantum dots are unique class of semiconductor because they are so small, as such they have atom-like behavior and enable the study of quantum mechanical effects on a length scale that is around 100 times larger than the pure atomic scale. At these small sizes materials behave differently, giving quantum dots unprecedented tuning ability and enabling never before seen applications to science and technology. Rapid progress in nanofabrication technology has made possible the growth of various nano-scale devices where both the atomicity and quantum-mechanical effects play a critical role in determining the overall device characteristics. This leads to a considerable challenge in modeling these devices[52]. The Figure 1.2 (a) shows a localization of electrons and quantization of energy levels in an atom and Figure 1.2 (b) shows the physical structure Quantum Dot. The physical structure of Quantum Dot can be understood as a well conducting/ low energy domain, where the domain size is in nm. The Quantum Dots has quantized energy levels and countable number of electrons in it, which makes it to sound like an artificial atom.
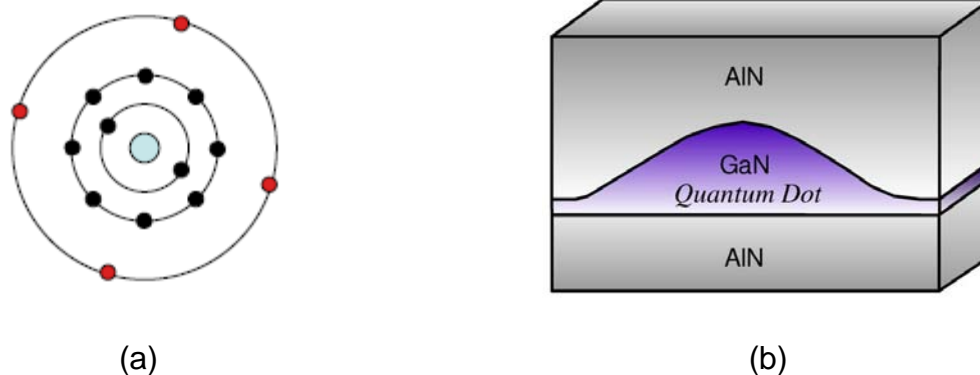
Figure 1.2 (a) shows localization of electrons in an atom and (b) shows the physical structure of an AlN/GaN Quantum dot

1.3.1 Market Analysis

The [53] global market for quantum dot (QD) technology generated an estimated $28.6 million in 2008. This is expected to increase at a compound annual growth rate (CAGR) of 90.7% to reach $721.1 million in 2013. QDs in the optoelectronics sector are expected to have the largest market share in 2013, worth $245.7 million. Stand alone colloidal QDs were the only market sector in 2008, worth $28.6 million. This is expected to increase at a CAGR of 30% to reach $106.1 million in 2013[53]. Evident Technologies, a New York based company is one of the pioneers in commercializing Quantum Dots for day to day applications. Their applications are in the field of displays, LED's, thermoelectric, life sciences, photonics and solar cells. The tunable bandgap of EviDots allows Evident Technologies to create products with unique optical and electronic properties and a broad range of emission frequencies.
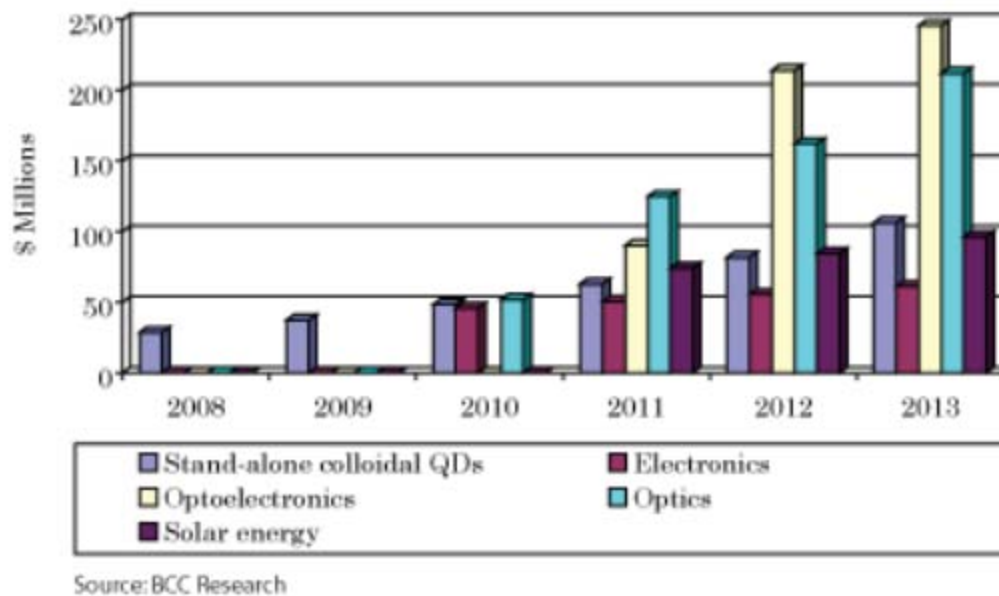
Figure 1.3 Global Market growths for Quantum Dots in promising commercial market sector, 2008 – 2013, from Ref[53].

1.4 ENERGY QUANTIZATION IN QUANTUM DOTS

Similar to that of the atoms in any crystal structure, the electrons in quantum dots have a range of energies. The concepts of energy levels, bandgap, conduction band and valence band still apply. However, there is a major difference between the bulk semiconductors and the quantum dots i.e. the electrons in bulk (much bigger than 10 nm) semiconductor material have range of energies. One electron with a different energy than a second electron is described as being in a different energy level, and it is established that only two electrons can fit in any given level. In bulk, energy levels are very close together, so close that they are described as continuous, meaning there is almost no energy difference between them. Average physical separation between the electron and hole is referred to as the Exciton Bohr Radius; this physical distance is different for each material. In bulk, the distance between electron and hole is

much larger than the Exciton Bohr Radius, allowing the exciton to extend to its natural limit. However, if the size of a semiconductor crystal becomes small enough that it approaches the size of the material's Exciton Bohr Radius, then the electron energy levels can no longer be treated as continuous - they must be treated as discrete, i.e. there is a small and finite separation between energy levels. This situation of discrete energy levels is called quantum confinement, and under these conditions, the semiconductor material ceases to resemble bulk, and instead can be called a quantum dot. This has large repercussions on the absorptive and emissive behavior of the semiconductor material [55].

Since quantum dots have discrete energy levels rather than continuous energy levels, the addition or subtraction of just a few atoms to the quantum dot has the effect of altering the boundaries of the bandgap. Even the Change in geometry of the surface of the quantum dot also changes the bandgap energy; this is due to the small size of the dot, and the effects of quantum confinement. The bandgap in a quantum dot will always be energetically larger; therefore, we refer to the radiation from quantum dots to be "blue shifted" reflecting the fact that electrons must fall a greater distance in terms of energy and thus produce radiation of a shorter and therefore "bluer" wavelength. However, with quantum dots, the size of the bandgap is directly proportional to the size of the dot. Because the emission frequency of a dot is dependent on the bandgap, it is therefore possible to control the output wavelength of a dot with extreme precision [55].

1.5 MOTIVATION BEHIND QUANTUM DOTS

Quantum [54] dots are particularly significant for optical applications due to their theoretically high quantum yield. In electronic applications they have been proven to operate like a single-electron transistor and show the Coulomb blockade effect. Being zero dimensional, quantum dots have a sharper density of states than higher-dimensional structures. As a result, they have superior transport and optical properties, and are being researched for use in diode lasers, amplifiers, and biological sensors. Figure 1.3 illustrates the 1-Dimensional representation of a Quantum Dot with presence of different energy levels also represented in 1-Dimension (green dashes). The red arrows inside the potential wells indicate the direction of electron motion i.e. from one energy level to another energy level.
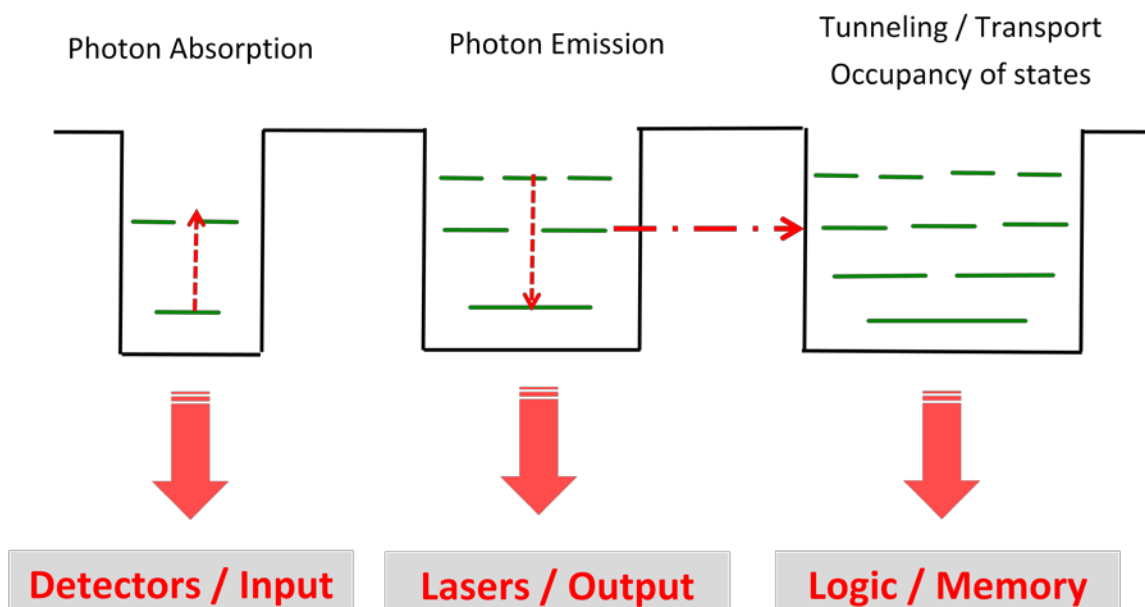
Figure 1.4 shows the potential for Quantum Dots to exhibit both optoelectronic and electronic properties.

In Figure 1.4 when an electron moves from lower energy level (S-level) to next higher energy level (P-level), and if we are able to detect the presence of an charge or electron in the exited energy level, it forms a optical detector. If we are able to pump electrons from higher energy level (P-level) to lower energy level (S-level), with emission of a photon it gives rise to optical devices like Lasers and LEDs.

1.6 APPLICATIONS

Quantum dots have also been suggested as implementations of qubit for quantum information processing. The ability to tune the size of quantum dots is advantageous for many optoelectronic applications.

1.6.1 Memory

Quantum Dots when used in electronic applications can be modeled to show coulomb blockade effect. The simplest device in which the effect of Coulomb blockade can be observed is the so-called single electron transistor. It consists of two tunnel junctions sharing one common electrode with a Quantum Dot at the channel region, known as the *island*. The electrical potential of the island can be tuned by a third electrode (the *gate*), capacitively coupled to the island. Here the electron hops from source to island and then to drain. This can be used in memory applications. The image from Scanning Electron Microscope is shown in Figure 1.5 (a).

1.6.2 Optoelectronic Devices

Quantum dots are valued for displays, because they emit light in very specific Gaussian distributions. This can result in a display that more accurately renders the colors that the human eye can perceive. Quantum dots also require very little power since they are not color filtered. Quantum Dots provide display technology which differs from cathode ray tubes (CRTs), liquid crystal displays (LCDs), but it is similar to organic light-emitting diode (OLED) displays, in that light is supplied on demand, which is enabling mobile devices with longer battery lives. Quantum dots of lead selenide can produce as many as seven excitons from one high energy photon of sunlight. Quantum dot photovoltaic devices would theoretically be cheaper to manufacture, as they can be made "using simple chemical reactions [54]. Due to the tight confinement of charge carriers in quantum dots, they exhibit an electronic structure similar to atoms. Lasers fabricated from such an active media exhibit device performance that is closer to gas lasers [56]. Figure 1.5 (d) shows an example of Quantum Dot Laser.

Another major advantage of Quantum Dots is that they can receive light from any angle or in other words they have weak incident angle dependence when compared to that of the quantum well structures. Quantum Dots have built in anisotropy and state quantization in all 3 dimensions which eliminates the need for gratings. Figure 1.5 (b) shows the structure of a Quantum Dot photo detector and an incident angle dependence graph comparing Quantum Dots and quantum well structures. Since their size is less than that of wavelength of visible

light, it eliminates many scattering losses. Quantum dots also require very little power since they are not color filtered.

1.6.3 Quantum Computer

Quantum dot technology is one of the most promising candidates for use in solid-state quantum computation. Quantum computers are different from traditional computers based on transistors. The basic principle behind quantum computation is that quantum properties can be used to represent data and perform operations on these data. The normal computers operates based on bits (0 or 1) but the quantum computers operates based on qubit (0 or 1 or superposition of 0 and 1), so a quantum computer can have multiple states. If a normal computer can do 1 work at a time, a quantum computer will be able to perform 1 million processes in the same time. Figure 1.5 (c) shows the Bhor's sphere representing a qubit.

1.6.4 Colloidal Markers

Cadmium Selenoid (CdSe) and Zinc Selenoid (ZnSe) Quantum Dots exhibit fluorescence when exposed to UV rays, these are called Colloidal Dots. These Colloidal Dots are used in the field of medicine to detect cancer. Research is going on to add chemicals to these Colloidal Dots which can attach themselves to cancer cells and then shine light on them to detect the cancer cells. Figure 1.5 (e) shows various color Colloidal Dots exhibiting fluorescence.
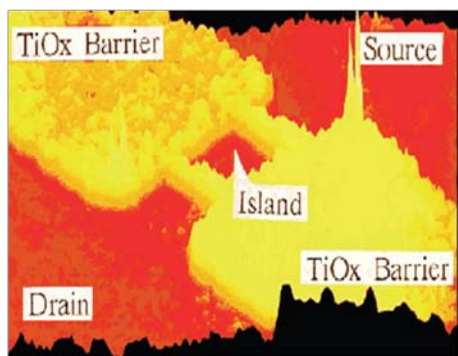
(a) Harris @ Stanford : Single electron transistor
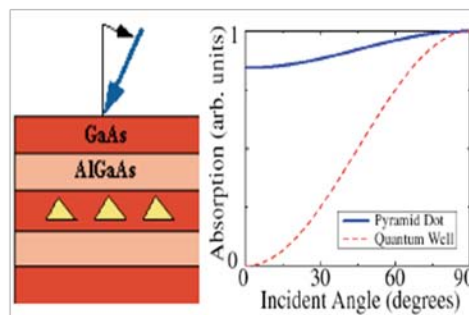
(b) Quantum Dots: Absorption has weak incident angle dependence
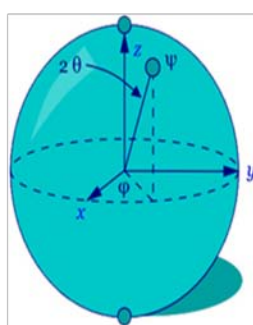
(c) Bloch sphere
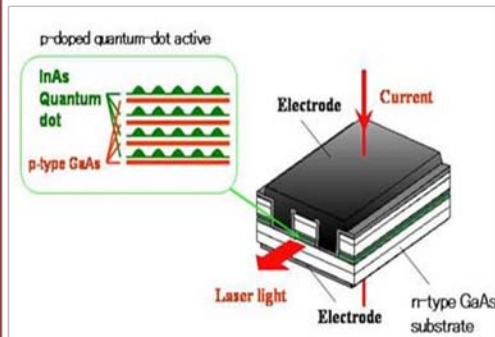
(d) Quantum Dot Laser
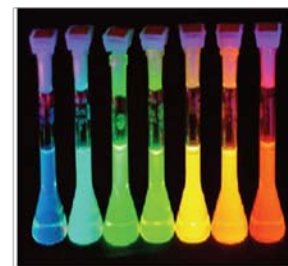
(e) Colloids used as medical markers

Figure 1.5 shows various applications of Quantum Dots

1.6.5 Quantum Dot Cellular Automata (QCA)

QCA is a revolutionizing concept that completely changes the way we have been thinking about circuits. It has a cell containing 4 Quantum Dots with 2 electrons/charges in them which can tunnel through the Quantum Dots. This is represented schematically in Figure 1.6 below.
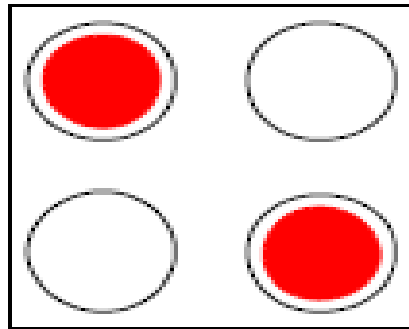
Figure 1.6 Schematic of Quantum Dot Cellular Automata

The Coulombic coupling between the electrons in the Quantum Dots polarizes them in 1 direction. Based on the direction of polarization a specific bit value is assigned (Polarization $P = -1$, Bit Value = 0 and Polarization $P = 1$, Bit Value = 1). The polarization is represented in Figure 1.7
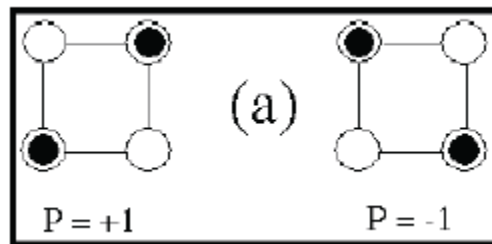
Figure 1.7 shows QCA polarization

Based on the above logic basic logic gates are constructed. Figure 1.8 shows schematic of Majority Gate which implements the AND & OR logic. The figure also shows a truth table for the majority gate.
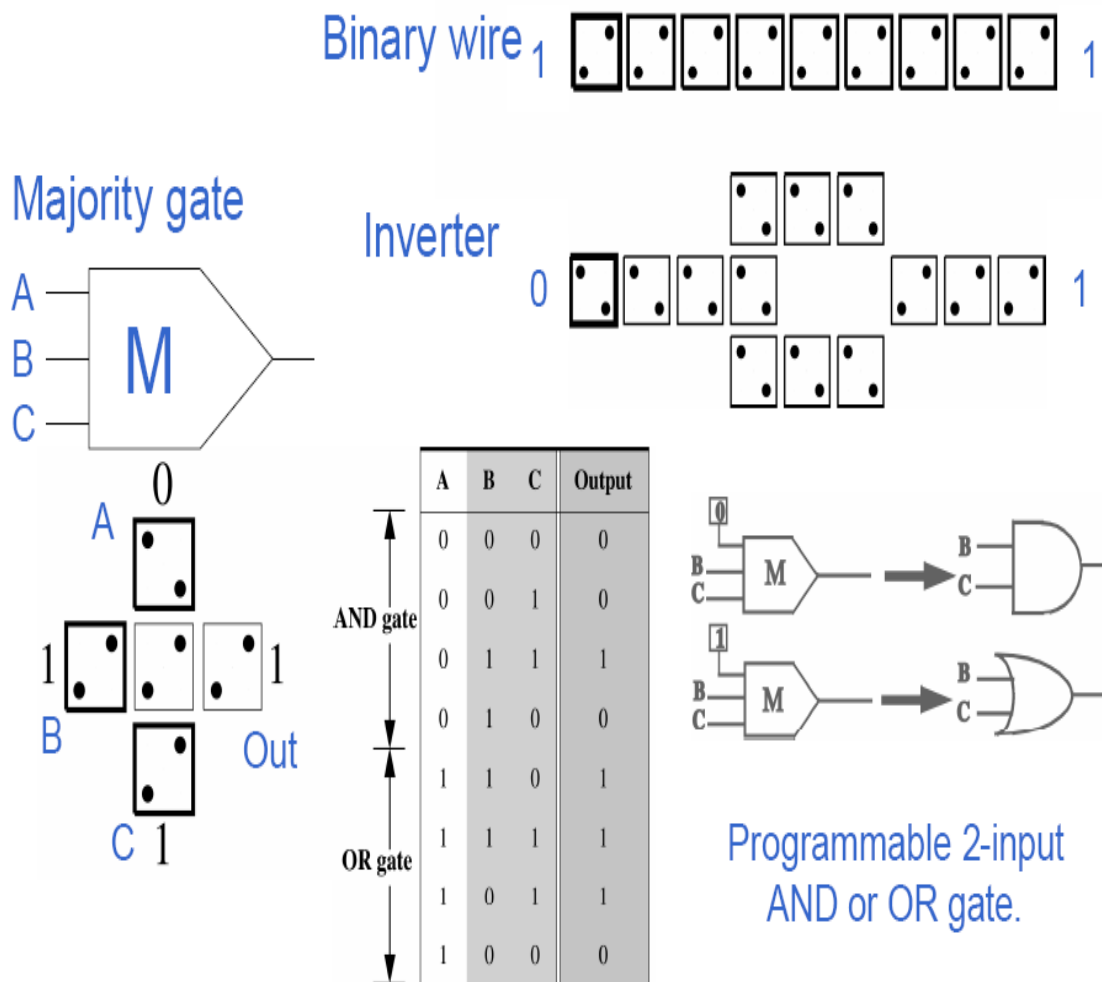
Figure 1.8 shows Majority gate implementing AND, OR logic with its Truth Table, it also shows the schematic of binary wire and inverter.

1. 7 ISSUES IN QUANTUM DOTS

The [52] *lack of structural symmetry* in the overall geometry of the nanodevices usually requires explicit three-dimensional representation. For example, Stranski-Krastanov growth techniques tend to produce self-assembled InAs/GaAs quantum dots (QDs) with some rotational symmetry, *e.g.* disks, domes, or pyramids. These structures are generally not perfect geometric

objects, since they are subject to interface inter-diffusion and discretization on an atomic lattice. There is no such thing as a round disk on a crystal lattice. Therefore, the underlying crystal/atomistic asymmetry imposes immediate restrictions on the realistic geometry and demands a full atomistic treatment.

Theoretical modeling of higher order piezo electric terms must be advocated. Generally quantum dots have focused exclusively on the first-order piezoelectric tensor, neglecting possible higher-order terms and their effects.

Quantum dots *require better modeling approach*. Continuum and ab initio models fail to take into account the effect of (1) interface potential (2) strain relaxation (3) Peizo & Pyro electric effects. Hence requires atomistic modeling approach.

1.8 HIGH ELECTRON MOBILITY TRANSISTORS (HEMT)

Quantum well structures have attracted the attention of device engineers and device designers due to its ability to segregate impurities from the carriers in these structures and thereby realize large carrier concentration without associated reduction in mobility. The larger conductivity resulting from the large carrier concentration and larger mobility was expected to give higher switching speed and transconductance. This expectation has been satisfied by High Electron Mobility Transistor (HEMT), also called as Two-Dimensional Electron Gas Field Effect Transistor (TEGFET) or Modulation Doped Field Effect Transistor (MODFET) or Selectively Doped Field Effect Transistor (SDFET) [14]. Since the demonstration of the first GaN-based transistors, rapid progress has

been made in their development and novel III–N high-electron mobility transistor (HEMT) devices have been proposed [15].

1.8.1 Market Analysis

The technology of HEMT's has reached the stage of commercial exploitation. As the market for cellular, personal communications services, broadband access are expanding and third-generation (3G) mobile systems coming closer to reality, RF & Microwave power amplifiers are beginning to be the focus of attention. Variety of power amplifier technologies are vying for market share like Si-LDMOS (Lateral-diffused MOS) and Bipolar transistors, GaAs MESFETs, GaAs (or GaAs/InGaP) hetero-junction bipolar transistors (HBTs),SiC (Silicon Carbide) MESFETs and GaN HEMTs [17]. The need for high power, high frequency transistors is increasing steadily, commensurate with the huge demand for wireless telecommunications. As wireless communication data rates continue to become increasingly faster, power consumption in base stations is also increasing. GaN HEMTs are promising devices to realize lower power consumption for high-power amplifiers in next-generation, high-speed wireless communication systems. But they must maintain high reliability—a long lifespan—to withstand harsh usage conditions, including high temperatures and high drain voltages. Fujitsu has emerged with an advanced GaN HEMT, which offers transistors to operate even at 200°C for more than 1 million hours under pinch-off condition with a drain voltage of 50V, offering the world's longest lifecycle for GaN HEMTs.

The high voltage feature of GaN HEMT eliminates the need for voltage conversion. Commercial systems (e.g. Wireless Base Station) operate at 28 Volts and a low voltage technology would need voltage step down from 28 V to the required voltage. However, GaN devices can operate potentially up to 42 Volts. The higher efficiency that results from this high operating voltage reduces power requirements and simplifies cooling, an important advantage, since cost and weight of cooling systems is a significant fraction of the cost of a high power microwave transmitter. The rate of progress in the power density and total power available from AlGaN/GaN HEMTs has been remarkable as shown in Figure below[17].
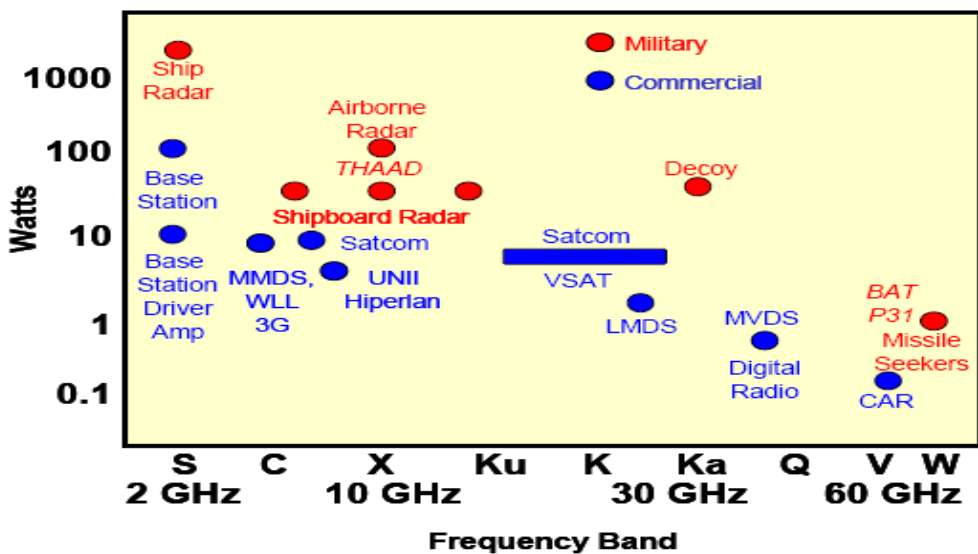
Figure 1.9 High frequency applications of GaN HEMT in various sectors, from Ref[17].

1.9 PURPOSES AND OUTLINE OF THIS THESIS

The focus of this work is majorly dedicated to effects of internal fields on Quantum Dots (QD) and also a small study of major reliability concern due to effects of internal fields on HEMT structures.

The purpose of this thesis work is to study the effects of internal fields (piezo and pyro strain) due to heterojunction structure in two types of Quantum Nano structures namely, Quantum Dots and HEMTs. For this purpose we use the atomistic NEMO-3D simulator to study the effect of internal fields in both Quantum Dots and HEMTs. In this work we first discuss about the effect of internal fields in Zincblende Quantum Dots and AlN/GaN HEMTs.

1.9.1 Effect of internal fields in Zincblende Quantum Dots

Built-in [52] electrostatic fields in Zincblende quantum dots originate mainly from—(1) the fundamental crystal atomicity and the interfaces between two dissimilar materials, (2) the strain relaxation, and (3) the piezoelectric polarization. In this work, we use the atomistic NEMO 3-D simulator to study the origin and nature of the internal fields in InAs/GaAs quantum dots with *three* different geometries, namely, box, dome, and pyramid. We then calculate and delineate the impact of the internal fields in the one-particle electronic states in terms of shift in the conduction band energy states, anisotropy and twofold degeneracy in the *P* level, and formation of mixed excited bound states. Models and approaches used in this study are as follow: (1) Valence force field (VFF) with strain-dependent

Keating potentials to calculate *atomistic* strain relaxation; (2) 20-band nearest-neighbor $sp^3d^5s^*$ tight-binding model for the calculation of single-particle energy states; and (3) For piezoelectricity, for the first time within the framework of $sp^3d^5s^*$ tight-binding theory, *four* different recently-proposed polarization models (linear and non-linear) have been considered in conjunction with an atomistic 3-D Poisson solver that also takes into account the image charge effects. Specifically, in contrast to recent studies on similar quantum dots, our calculations yield a *non-vanishing* net piezoelectric contribution to the built-in electrostatic field. Demonstrated also is the importance of full three-dimensional (3-D) *atomistic* material representation and the need for using *realistically-extended* substrate and cap layers (systems containing ~2 million atoms) in the numerical modeling of these reduced-dimensional quantum dots [52].

1.9.2 Effect of internal fields in HEMT's

In this work, we use the atomistic NEMO 3-D simulator to study the origin and nature of the internal fields in AlN/GaN HEMTs. Here we calculate the Peizo and Pyro strain using NEMO 3D and then use 3D Poisson solver to calculate the potential. Finally a T-CAD simulator, SILVACO is employed to model the AlN/GaN device. Tony-Plot is used to plot the I –V characteristics. The device channel region considered in this work is illustrated in the Figure 1.10.

| GaN cap (~1 nm) |
| AlN (3.5 nm) |
| GaN undoped (2 µm) |
| AlN buffer |
| Sapphire |
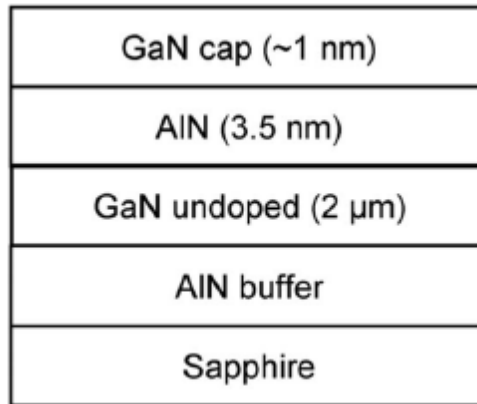
Figure 1.10 Layer Structure of an AlN/GaN HEMT grown on Sapphire, from Ref [21]

In Chapter 1, a brief introduction to semiconductor industry is given. It also discusses the era of FET especially MOSFET, where we see Moore's law is facing a serious concern. In the later part of the chapter we discuss about the Evolution of Quantum Dots and HEMTs, their current market trend, the issues in these quantum structures and the purpose of this document.

In Chapter 2, we discuss about the effect of internal fields on Quantum Dots, Where we discuss the influence of strain on the band structure, electrostatic potential landscape and overall device characteristics. It also discusses about the various models that captures these strain effects on these quantum devices. We also discuss about the transport properties of HEMTs and the effect of strain on them.

In Chapter 3, we discuss about the various modeling and design tools that are employed in this work to study the effect of strain on these quantum device structures. We explore in detail about the NEMO 3D, an atomistic device simulator, which is used to capture the strain effects.

Chapter 4 displays the results obtained from simulation. Here we discuss the results obtained in our study and summarize our findings in the conclusion.

CHAPTER 2

BUILT IN FIELDS AND THEIR EFFECTS ON QUANTUM NANO STRUCTURES

Hetero-epitaxially grown GaAs/GaN tends to have structural defects arising due to mismatch in lattice parameters and different thermal expansion coefficients between the GaAs/GaN and AlGaAs/AlN layer. These structural defects in turn will induce built in fields, which affects these Quantum Nano structures. Hence this necessitates us to know about the built in fields and their effect on these Quantum Nano structures.

.

2.1 BUILT IN FIELDS

Built in fields or internal fields is result of 3 major effects originating from the lattice-mismatched semiconductors. In the case of the InAs/GaAs quantum dots, the lattice mismatch is around 7% which exhibits very high internal fields. (1) *Interface Potential:* When lattice mismatched hetero junction materials are fabricated, there exists a asymmetry in the lattice atoms, which gives rise to a potential called interface potential. In Figure 2.1 (a) the lattice mismatch between InAs and GaAs materials are shown. (2) *Strain Relaxation:* When lattice mismatched materials are grown on top of each other the atoms try to make bonds despite the variation in the lattice constant between various materials, this gives rise to strain. But according to laws of equilibrium, always any element in nature tries to remain in the lower energy state or in equilibrium. Hence the strain formed due to the hetero-junction spreads through the material causing strain relaxation. Due to strain relaxation the material surface undergoes

reconstructions. Since the strain relaxation is time dependent, these surface reconstructions are also time dependent, hence molecular dimension simulations are required to capture these effects. Figure 2.1(b) shows the surface reconstruction of InAs material after strain relaxation. (3) *Piezoelectric Polarization:* Piezoelectricity is defined as conversion of mechanical strain to electrical energy. Due to the presence of strain in the hetero-junction materials, they tend to exhibit piezoelectricity and the polarization caused due to this piezoelectricity is called piezoelectric polarization. Always the effect tends to oppose its cause; similarly here the piezoelectric polarization is opposed by strain relaxation. The summations of all 3 above effects are called built in fields or internal fields. These built in fields affect the overall device characteristics of quantum dots. Hence again there is an emphasis on 3 dimensional atomistic modeling.
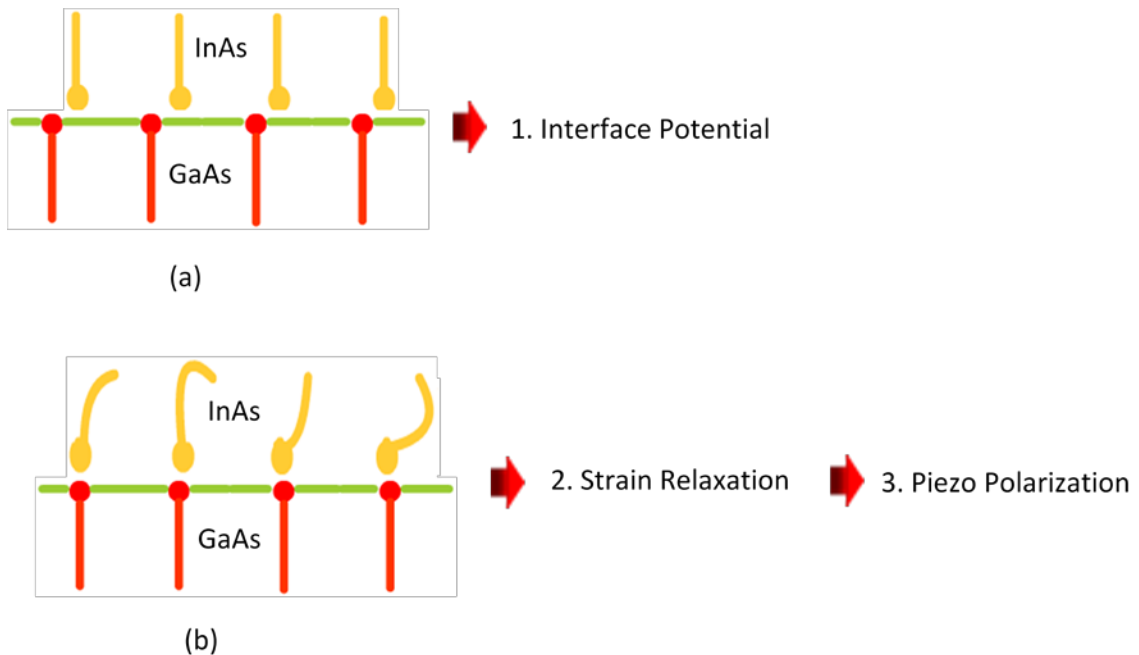
Figure 2.1 (a) shows the lattice mismatch between InAs and GaAs materials (b) shows the surface reconstruction of InAs material after strain relaxation.

2.2 NEEDS TO MODEL EFFECTS OF BUILT IN FIELDS IN QUANTUM DOTS

Figure 2.2 (a) shows the conduction and valance band energy states, with the first 2 energy levels (S and P levels) with wave vector on them for an ideal Quantum Dot. When we consider the above mentioned ideal case for applications in Quantum Dot LEDs, we see that the maximum numbers of exiton pairs are formed or in other words there is a maximum overlap between the wave vectors which is directly proportional to the intensity of the light emitted by the LED. The band gap E_g between the S levels of the conduction and valance band also contribute to define the color of the LED. Figure 2.2 (b) shows a change in potential profile in the conduction band due to the effect of built in fields. This change in potential profile is taken into account in Figure 2.2 (c), where there is a shift in the S energy level is graphically represented. Here again when we put

this above condition for LED applications we find there is very low light intensity produced due to minimum or less overlap of wave vectors of the 2 S energy levels. We also see there is a change in bandgap E_g which prohibits us from obtaining the desired color in LED. Hence this study necessitates the need to take into account the effect of internal fields into consideration when modeling Quantum Dots.

Figure 2.2 (a) shows the conduction and valance band energy states, with the first 2 energy levels (S and P levels) with wave vector on them for an ideal Quantum Dot. (b) Shows a change in potential profile in the conduction band due to the effect of built in fields. (c) Shows Quantum Dots under real time conditions.

2.3 EFFECT OF STRAIN IN QUANTUM DOTS
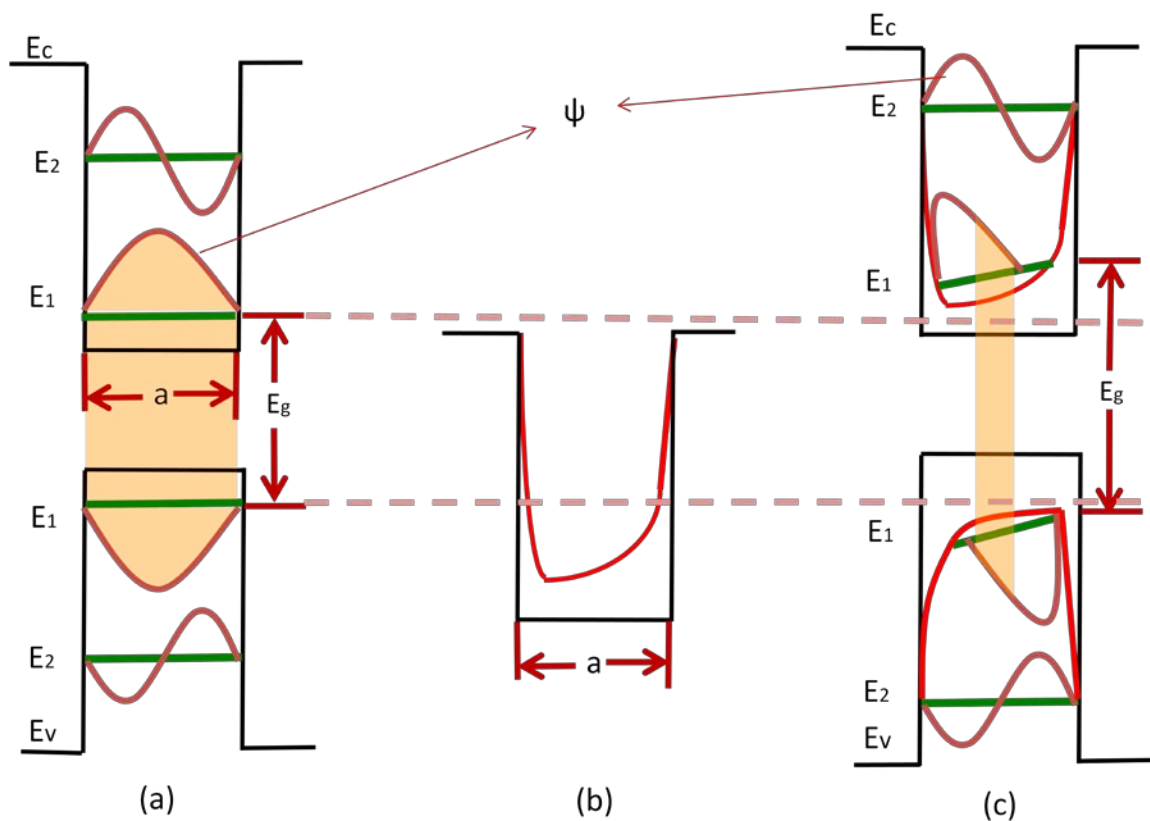
Strain [52] originates from the assembly of lattice-mismatched semiconductors and, in the Stranski-Krastanov growth mode, indeed drives the creation of the QDs. In the case of the InAs/GaAs quantum dots, the lattice mismatch is around 7% and leads to a strong *long-range* strain field within the extended neighborhood of each quantum dot [3]. Strain can be atomistically inhomogeneous, involving not only *biaxial* components but also non-negligible *shear* components. Strain in reduced dimensional structures strongly influences the core and barrier material band structures, modifies the energy bandgaps, and further lowers the underlying crystal symmetry. In the nanoscale regime, the classical harmonic linear/continuum elasticity model for strain, which can capture strain only on a mesoscopic scale, is clearly inadequate [4][5], and device simulations must include the fundamental quantum character of charge carriers and the long-ranged atomistic strain effects with proper boundary conditions on an equal footing.

A variety of III-IV materials such as GaAs, InAs, GaN, are *piezoelectric.* Any spatial non-symmetric distortion in nanostructures made of these materials will create piezoelectric fields, which will modify the electrostatic potential landscape. Recent spectroscopic analyses of self-assembled QDs demonstrate polarized transitions between confined hole and electron levels[2]. While the continuum models (effective mass or $k \bullet p$) can reliably predict aspects of the single-particle energy states, they fail to capture the observed non-degeneracy and optical anisotropy of the excited energy states in the (001) plane. These methods fail

because they use a confinement potential which is assumed to have only the

structural symmetry of the nanostructure, and they ignore the underlying crystal

asymmetry. The experimentally measured symmetry is significantly lower than

the assumed continuum/shape symmetry mainly because of underlying

crystalline atomicity and interfaces, strain relaxation, and the piezoelectric fields.

For example, in the case of pyramidal QDs with square bases, continuum models

treat the underlying material in C_{4v} symmetry while the atomistic representation

lowers the crystal symmetry to C_{2v} [2]. QDs with circular bases having structural

C_∞ symmetry also exhibit optical polarization anisotropy due to the atomistic

asymmetry and the built-in electrostatic fields induced in the underlying lattice.

2.4 EFFECT OF STRAIN ON TRANSPORT PROPERTIES

There is a great deal of interest in pseudomorphic HEMT due to its high

carrier density, which has been made possible by the presence of narrower

bandgap strained channel. The effect of uniaxial strain produced by mismatched

epitaxy on the valance band is quite profound, hence a compressive strain in

growth plane can reduce the in plane hole effective mass, thus offering an

improved performance of p-type devices [29]. Let us get into detail about various

strains caused due to lattice mismatched epitaxy.

2.5 EFFECT OF INETRNAL FIELDS ON HEMTs

Two dimensional electron gases in $Al_xGa_{1-x}N/GaN$ based heterostructures,

suitable for high electron mobility transistors, are induced by strong polarization

effects [30]. The sheet carrier concentration and the confinement of the two dimensional electron gases located close to the AlGaN/GaN interface are sensitive to these polarization effects. Piezoelectric effects exert a substantial influence on the concentration and distribution of free carriers in strained group-III nitride heterostructures with the wurtzite crystal structure [31][32][33]. Piezoelectric polarization of the strained AlGaN or AlN /GaN barrier layer is more than five times that of AlGaAs/ GaAs structures. The high sheet carrier concentration and narrower confinement of the 2DEG is achieved due to polarization induced electric fields, but in addition to the high piezoelectric polarization, the spontaneous polarization (polarization at zero strain) is very large in wurtzite group-III nitrides, increasing from GaN over InN to AlN,(n21) resulting in a further increase of polarization induced effects in AlGaN or AlN / GaN based HEMTs [30]., E.g. Group III wurtzite N-face heterostructures showcases highest 2DEG mobility of 1150 (300 K) and 3450 cm^2/V s (77 K) was achieved for a 400 Angstrom thick undoped barrier with an Al concentration of x = 0.25, causing an electron sheet carrier concentration of 5 x $10^{12}cm^{-2}$ at the GaN/AlGaN interface. The sheet carrier concentration in the channel induced by polarization charges is determined self-consistently from a coupled Schrodinger and Poisson equation solver for pseudomorphic HEMT structure.

The piezo and pyro strains are calculated using atomistic NEMO-3D simulator in this literature. To solve Poisson equation self consistently we use a 3 dimensional Poisson solver. The Next chapter details about the modeling software used in this thesis.

CHAPTER 3

MODELLING & DESIGN TOOLS

3.1 NEED FOR SIMULATORS OR MODELLING TOOLS

Simulation is playing key role in device development today. Device simulation tools simulate the electrical characteristics of semiconductor devices, as a response to external electrical, thermal or optical boundary conditions imposed on the structure. There are two major issues of concern. Product cycles are getting shorter with each generation, and the demand for production wafers shadows development efforts in the factory. While simulations may not be completely predictive, they provide a good initial guess which ultimately reduces the number of iterations during the device development phase[39]. Besides offering the possibility to test hypothetical devices which have not yet been manufactured, device simulation offers unique insight into device behavior by allowing us to observe internal phenomena that cannot be measured. Thus, a critical facet of the nano-devices development is the creation of simulation tools that can quantitatively explain or even predict experiments [39]. Now let us get into detail about the structure of this thesis and also about various modeling tools that are employed in this thesis.

3.2 MODELLING TOOLS USED

In this thesis, we use 3 different modeling tools each for a specific purpose, namely *NEMO 3D, 3D POISSON SOLVER &* a TCAD simulator *SILVACO.* To capture the strain that originates from the assembly of lattice-

mismatched semiconductors strongly modifies the energy spectrum of the
system, i.e. in our case its AlGaAs/GaAs in QDs and AlN/GaN interface HEMTs.
In order to calculate the strain we use an atomistic device simulator knows as
NEMO 3D. NEMO-3D is a nano-electronic modeling tool that analyzes the
electronic structure of nanoscopic devices. Once we obtain the strain values, we
calculate the potential due to strain or in other words the built in voltage caused
due to strain, using a *3Dimensional Poisson Solver.* This Poisson solver solves
the 3 dimensional Poisson equation to obtain the potential. On obtaining the built
in potential, we add it to the applied potential and solve the Schrödinger equation
self-consistently to obtain the Energy Landscape (E) and Wave Function (Ψ). To
solve the Schrödinger equation self-consistently, we again use the atomistic
device simulator *NEMO 3D.* In order to design the pHEMT of specific dimensions
and to study its electrical characteristics such as $I_d V_g$, $I_d V_d$ characteristics, we
use a Technology Computer-Aided Design (TCAD) software known as *SILVACO.*
We input the Energy Landscape (E) values obtained from NEMO 3D, into
SILVACO to study the change in electrical characteristics due to the effect of
strain.

3.2.1 Modeling Quantum Dots

In [52] the case of quantum dot simulations, the simulation domain
requiring multimillion atoms prevents the use of *ab initio* methods.
Empirical methods (*Pseudopotentials* [2] [8] and *Tight Binding* [9]), which
eliminate enough unnecessary details of core electrons, but are finely

tuned to describe the atomistically dependent behavior of valence and conduction electrons, are attractive in realistically-sized nanodevice simulations. Tight-binding is a local basis representation, which naturally deals with finite device sizes, alloy-disorder and hetero-interfaces and it results in very sparse matrices. The requirements of storage and processor communication are therefore minimal compared to pseudopotentials and implementations perform extremely well on inexpensive Linux clusters.

3.3 NEMO 3D

NEMO 3-D bridges the gap between the large size, classical semiconductor device models and the molecular level modeling [39]. Novel nano-electronic devices such as quantum dots, nanowires, and ultra-scaled quantum wells are expected to significantly enhance existing nanoelectronic technologies. The behavior of carriers and their interaction with their environment need to be fundamentally explained at a quantum mechanical level. Most of these device level descriptions utilize an effective mass approach where the concepts of device and material meet at the nanometer scale. A representation of the constituent materials at the atomic resolution is needed to quantitatively model devices with a countable number of atoms [40]. This approach is explained in the Figure 3.1 below.
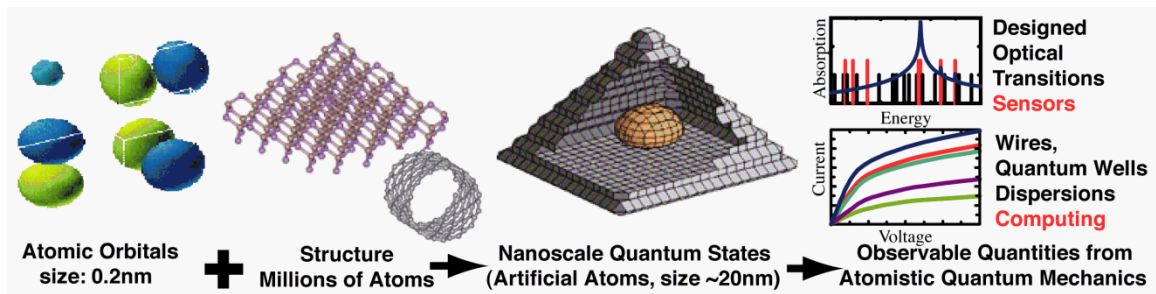
Figure 3.1 Explains NEMO 3-D modeling agenda: map electronic properties of individual atoms into realistic structures containing millions of atoms, computation of nanoscale quantum dots that maps into real applications, from Ref [39][40].

NEMO 3-D enables the computation of atomistic (non-linear) strain and piezoelectric field for over 64 million atoms and of electronic structure for over 52 million atoms, corresponding to volumes of $(110nm)^3$ and $(101nm)^3$, respectively. Excellent parallel scaling up to 8192 cores has been demonstrated[14]. We are not aware of any other semiconductor device simulation code that can simulate such large number of atoms. NEMO 3-D includes spin in its fundamental atomistic tight binding representation. Effects of interaction with external electromagnetic fields are also included[52].

NEMO 3D currently allows calculating single-particle electronic states and optical response of various semiconductor structures including bulk materials, quantum dots, quantum wires, quantum wells and nano-crystals.

3.3.1 Components and Models

NEMO 3D [39] consists of 4 main components namely, Geometric Construction, Strain, Electronic Structure and Post processing of Eigen States.

(1) Geometric Construction: The purpose of Geometric Constructor is to represent the treated nanostructure in atomistic detail in the memory of the computer. It assigns each atom with three single-precision numbers representing its coordinates, information whether the atom is on the surface or in the interior of the sample, what kind of computation it will take part of (strain only or strain and electronic), and what its nearest neighbor relation in a unit cell. *(2) Strain*: The materials making up the Quantum Well nanostructure may differ in their lattice constants; for our case it is AlN/GaN. This lattice mismatch leads to the appearance of strain, due to which atoms throughout the sample are displaced from their bulk positions. Hence the computation of strain has become a necessary step in realistic simulations of these nanostructures. NEMO 3-D computes strain field using an atomistic valence force field (VFF) method with the Keating Potential. *(3) Electronic Structure:* The single-particle energies and wave functions are calculated using an empirical nearest-neighbor tight-binding model. Atoms are represented by the empirical tight binding model using s, sp3s*, or sp3d5s* models with or without spin. *(4) Post Processing of Eigenstates:* From the single-particle eigen-states various physical properties can be calculated in NEMO 3-D such as optical matrix elements [9], Coulomb and exchange matrix elements [39].

3.3.2 Parallel Implementation

The complexity and generality of physical models used in NEMO 3D places very high demands on computational resources. For example, in the 20-

band electronic calculation the discrete Hamiltonian matrix is of order 20 times the number of atoms. Thus, in a computation with 20 million atoms, the matrix is of order 400 million. Computations of that size can be handled because of the parallelized design of the package. In our work we use various parallel computers like Jaguar, Octopus etc for which NEMO 3D has been optimized. This super fast computer reduces the computational time to a greater extent.

3.3.3 Release and Deployment

NEMO 3-D was developed on Linux clusters at the Jet Propulsion Lab (JPL) and was released with an open source license in 2003. The originally released source is hosted at http://www.openchannelfoundation.org web site.

3.4 POISSON SOLVER (3D)

On obtaining the strain values using NEMO 3D, we need to calculate the built in potential by solving the Poisson equation self-consistently, the equation can be written as

$$\nabla^2 V_c(r) = -\frac{\rho}{\varepsilon}$$

(2.2)

The charge density **ρ** is the sum of doping charge, free charge and the quantum confined charge [29]. A simple FORTRAN code is written to solve the Poisson equation. The Poisson solver normalizes potential *V* with the thermal voltage *VT*, the carrier concentration with the intrinsic carrier concentration and the mesh with the intrinsic Debye length. It uses finite difference discretization to linearize the equation. *A* resultant matrix after the linearization procedure becomes diagonally

dominant which, in turn, leads to stable convergence. In order to run poisson solver we need to input the Spontaneous polarization constants (P_{sp}) and Peizoelectric polarization constant (e_{33}, e_{31} & e_{15}) which are obtained from the Table 3.1 below.

Table 3.1 Displays Lattice constants, spontaneous polarization, piezoelectric and dielectric constants of AlN, GaN and InN, from Ref [30].

Wurtzite	AlN	GaN	InN
a_0(Å)	3.112	3.189	3.54
c_0(Å)	4.982	5.185	5.705
c_0/a_0	1.601	1.627	1.612
	1.619 [a]	1.634 [a]	1.627 [a]
u	0.380 [a]	0.376 [a]	0.377 [a]
P_{SP}(C/m^2)	−0.081 [a]	−0.029 [a]	−0.032 [a]
e_{33}	1.46 [a]	0.73 [a]	0.97 [a]
(C/m^2)	1.55 [b]	1 [c]	...
		0.65 [d]	...
	1.29 [e]	0.63 [e]	...
e_{31}	−0.60 [a]	−0.49 [a]	−0.57 [a]
(C/m^2)	−0.58 [b]	−0.36 [c]	...
		−0.33 [d]	...
	−0.38 [e]	−0.32 [e]	...
e_{15}	−0.48 [b]	−0.3 [c]	...
(C/m^2)		−0.33 [d]	...
ϵ_{11}	9.0 [b]	9.5 [f]	...
ϵ_{33}	10.7 [b]	10.4 [f]	14.6 [g]

[a]Reference [43].

[b]Reference [44]

[c]Reference [45]

[d]Reference [46]

[e]Reference [47][48]

[f]Reference [49]

[g]Reference [50].

CHAPTER 4

RESULTS AND CONCLUSION

In this thesis, we study the effect of strain due to the presence of lattice mismatched hetero-junction materials, on Quantum Dots and the current characteristics of HEMT. In order to study this effect, we need to calculate the peizo and the pyro strains at the hetero-junction interface. In order to calculate the strain we use an atomistic device simulator knows as *NEMO 3D.* NEMO-3D is a nano-electronic modeling tool that analyzes the electronic structure of nanoscopic devices. Once we obtain the strain values, we calculate the potential due to strain or in other words the built in voltage caused due to strain, using a *3Dimensional Poisson Solver.* This Poisson solver solves the 3 dimensional Poisson's equation to obtain the potential. On obtaining the built in potential, we add it to the applied potential and solve the Schrödinger equation self-consistently to obtain the Energy Landscape (E) and Wave Function (Ψ). To solve the Schrödinger equation self-consistently, we again use the atomistic device simulator *NEMO 3D.*

4.1 SIMULATION RESULTS FOR QUANTUM DOTS

Figure 4.1 shows the simulated quantum dots having different geometries such as box, dome and pyramid. The InAs QDs grown in the [001] direction and embedded in a GaAs substrate used in this study have diameter/base length,

d~11.3 nm and height, *h*~5.6 nm, and are positioned on an InAs wetting layer of one atomic-layer thickness. The simulation of strain is carried out in the large computational box, while the electronic structure computation is restricted to the smaller inner domain; this is done to reduce the computational complexity. All the strain simulations fix the atom positions on the bottom plane to the GaAs lattice constant, assume periodic boundary conditions in the lateral dimensions, and open boundary conditions on the top surface. The inner electronic box assumes a closed boundary condition with passivated dangling bonds.
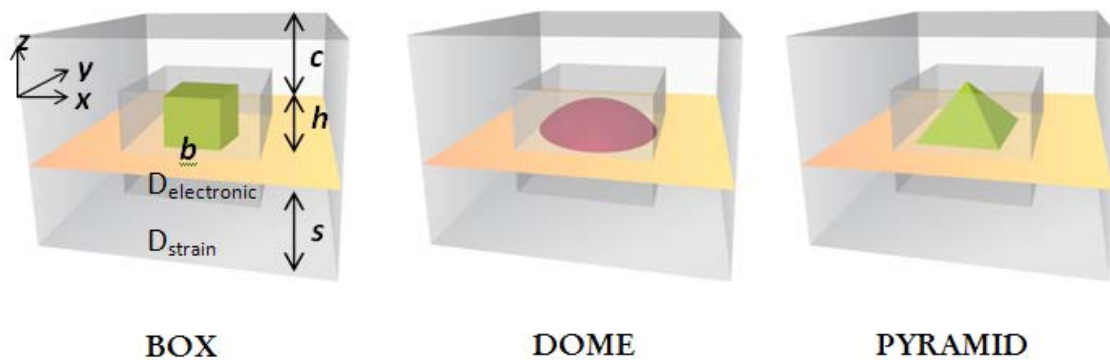

Figure 4.1 Simulated Box, Dome and Pyramid InAs/GaAs quantum dots on a thin (one atomic layer) InAs wetting layer. Two major computational domains are also shown. D_{elec}: central smaller domain for electronic structure (quantum) calculation, and D_{strain}: outer domain for strain calculation. In the figure: *s* is the substrate height, *c* is the cap layer thickness, *h* is the dot height, and *d* is the dot diameter/base length as appropriate.

Figure 4.2 shows the first four conduction band wavefunctions for each of the quantum dots *without* any strain relaxation and piezoelectricity. Both the InAs dot and the GaAs barrier assume the lattice positions of perfect Zincblende GaAs.

Here, the geometric shape symmetry is broken and the quantum dots, since constructed from atoms, have C_{2v} symmetries [2]. From the P level wavefunctions, it is understood from the figure that the crystal atomicity and the interfaces (between the dot material InAs and the barrier material GaAs) lower the geometric shape symmetry even in the absence of strain. The interface plane cannot be treated as a reflection plane [2] and there exist a short-range interfacial potential. However, it is important to note that the magnitude of the split (non-degeneracy) in the P level is largest in case of a dome dot (~7.39 meV) and minimum in a box (~1.2 meV). The anisotropy in the P level assumes opposite *orientations* for dome and pyramid dots. The first P state is oriented along [1$\underline{1}$0] ([110]) direction and the second along [110] ([1$\underline{1}$0]) direction in a dome (pyramid). Although the degeneracy is somewhat broken (~1.2meV) for a box the P states are almost isotropic.

BOX: $E_{1\underline{1}0} - E_{110} = 1.2$ meV

DOME: $E_{1\underline{1}0} - E_{110} = -7.39$ meV
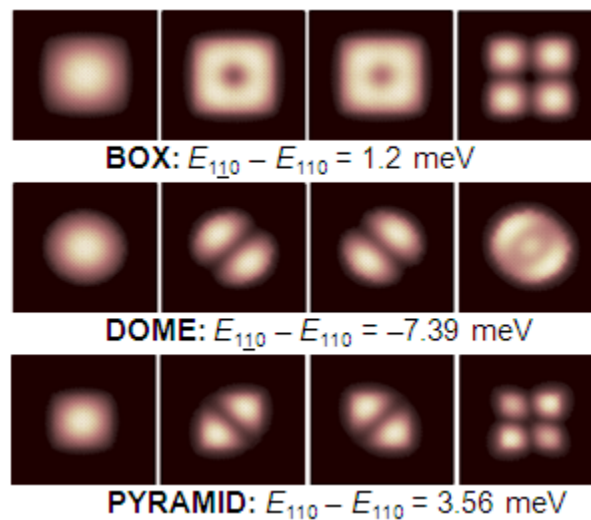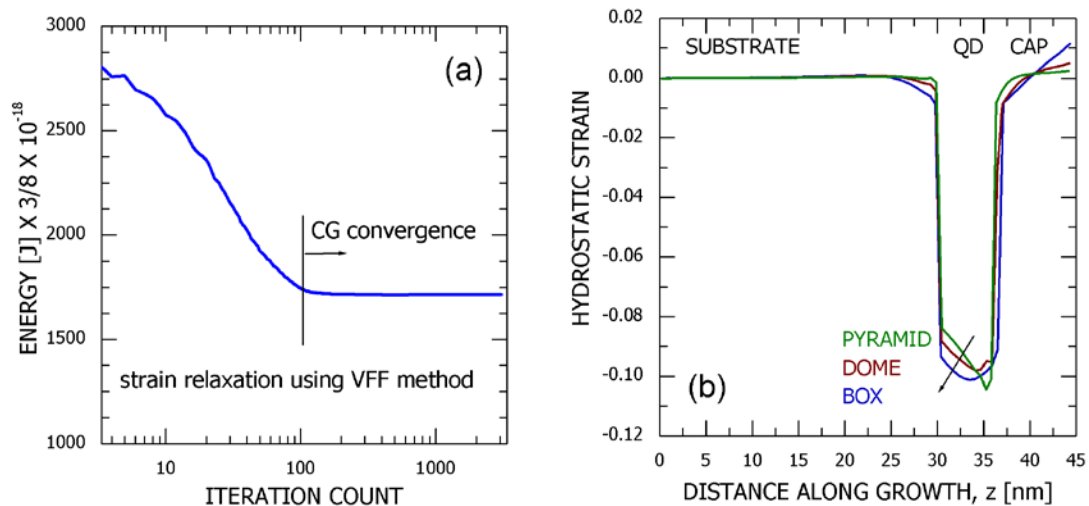
PYRAMID: $E_{1\underline{1}0} - E_{110} = 3.56$ meV

Figure 4.2 First four conduction band wave functions due to fundamental crystal and interfacial symmetry. Noticeable are the split (non-degeneracy) and the anisotropy (dominant in dome and pyramidal dots) in the P level.

Next, we introduce atomistic strain relaxation in our calculations using the VFF method with the Keating Potential. Here, the total elastic energy of the sample is computed as a sum of bond-stretching and bond-bending contributions from each atom. The equilibrium atomic positions are found by minimizing the total elastic energy of the system. However, piezoelectricity is neglected in this step. The total elastic energy in the VFF approach has only one global minimum, and its functional form in atomic coordinates is quadratic. The conjugate gradient minimization algorithm in this case is well-behaved and stable. *Figure 4.3a* shows the convergence characteristic in a typical simulation of atomistic strain relaxation of an InAs/GaAs quantum dot with ~1.8 millions of atoms. This demonstrates that the surface reconstructions are time dependent. Strain modifies the effective confinement volume in the device which distorts the atomic bonds in length and angles, and hence modulates the confined states. *Figure 4.3b* shows the trace of the hydrostatic strain distribution along the [001] direction for all three quantum dots (cut through the center of the dot). There are three salient features in this plot—(1) Atomistic strain is long-ranged and penetrates deep into both the substrate and the cap layers. However, there is a geometric dependence of spread is different in different-shaped quantum dots—largest in a box and minimum in a Pyramid. This is mainly due to the varying total volumetric pressure on to the surrounding material matrix. The spread of strain deep inside the surrounding material matrix not only stresses the importance of including enough of a substrate and cap layer to capture the long-range strain but

indicates opportunities to tune the energy spectrum with different capping layer thicknesses also. (2) In all three quantum dots, the hydrostatic strain has a non-zero slope within the quantum dot region. The presence of the gradient in the hydrostatic strain introduces unequal stress in the Zincblende lattice structure along the depth, breaks the equivalence of the [110] and [1$\underline{1}$0] directions, and finally breaks the degeneracy of the P level [2]. *Figure 4.3c* shows the wavefunction distributions for the first 4 (four) conduction band electronic states in a 2-D projection. However there is a pronounced optical anisotropy and non-degeneracy in the P level. It is also important to note that strain introduces uniform orientational pressure in all three quantum dots. For all three quantum dots, the first P state is oriented along the [110] direction and the second along the [1$\underline{1}$0] direction. *Figure 3c* also reveals the split/non-degeneracy in the P level (defined as $\Delta P = E_{1\underline{1}0} - E_{110}$) associated with each of the quantum dots. This value is found to be largest in a pyramid and minimum in a box.

(c)

BOX: $E_{1\underline{1}0} - E_{110} = 2.6$ meV

DOME: $E_{1\underline{1}0} - E_{110} = 5.9$ meV
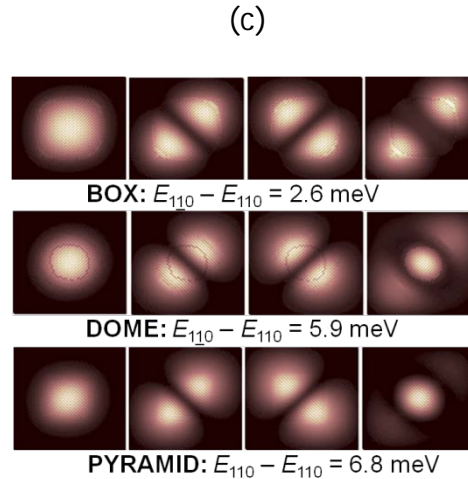
PYRAMID: $E_{1\underline{1}0} - E_{110} = 6.8$ meV

Figure 4.3 (a) Convergence of elastic energy in a typical simulation of InAs/GaAs quantum dot with ~2 million atoms. The total elastic energy of the sample is minimized using the conjugate gradient method. (b) Trace of atomistic hydrostatic strain along the growth ([001]) direction through the center in all three quantum dots. Diameter/base length, $d = 11.3$ nm, height, $h = 5.65$ nm, substrate thickness, $s = 30$ nm, and cap layer thickness, $c = 10$ nm. We see that strain penetrates deep into the substrate and the cap layers. Also, noticeable is the presence of gradient of strain inside the dot region that results in optical polarization anisotropy and non-degeneracy in the conduction band P level. (c) First 4 (four) electronic wave functions and split in the P levels in all three quantum dots including strain relaxation. Number of atoms simulated: 1.78 millions (strain domain), 0.8 million (electronic domain).

In pseudomorphically grown semiconductor heterostructures, the presence of

lattice mismatch results in a deformation in the crystal lattice and leads to a

piezoelectric field, which has been incorporated in the Hamiltonian as an external

potential (within a non-self consistent approximation) by solving the Poisson

equation on the Zincblende lattice. Traditionally, shear components of strain in

Zincblende crystals was considered to be the only source of piezoelectric. [2]

[14]. *Figure 4.4* shows the atomistic shear strain profiles in all three quantum dots. The off-diagonal strain tensors have the largest *magnitude* in the dome and minimum in the box shaped dots. However, it is important to note that the shear stress is maximally *spread* in a box dot (~22 nm within the substrate material), which also suggests that piezoelectric contribution would be largest in a box shaped quantum dot. The assumption that piezoelectric fields originate only from the *shear* components of the strain tensors is sometimes referred to as the *linear/first-order* treatment of piezoelectricity, which has recently been revised for InAs/GaAs quantum dots subject to the presence of enormous strain fields [18] [20]. Authors in Ref. [20] have calculated the piezoelectric properties of self-assembled Zincblende quantum dots using both linear and quadratic piezoelectric tensors that are derived from first-principles density functional theory. They have found that the previously ignored second-order term has comparable magnitude as the linear term and the two terms tend to oppose each other and cancel out. Inspired by this work, in our calculations, we included 4 (four) different models for piezoelectric polarization and they are as follow, (1) Linear/1st order term calculated using the experimental values. (2) Linear/1st order term from microscopically determined values (3) Quadratic/2nd order term using microscopically determined values.(4) Sum of 1st order and 2nd order using microscopically determined values The resulting piezoelectric potential distributions, corresponding to these 4 (four) different models, along the *Z* (growth) direction are shown in *Figure 4.5* for all three quantum dots. From this Figure, one can extract at least three important features—(1) Piezoelectric

potential has its largest *magnitude* in a pyramidal dot with the peak being located near the pyramid tip, and the minimum in a box. (2) As in the case of strain, the spread of the potential is largest in a box and minimum in a pyramid. (3) *Within the quantum dot region*, the second-order effect has comparable/similar magnitude as the first-order contribution, and, indeed, the two terms oppose each other. However, noticeable is the fact that the first-order contribution, as compared to the quadratic term, penetrates deeper inside the surrounding material matrix. This particular effect, we believe, in contrast to the findings in Ref. [20], results in a non-vanishing and reasonably large *net* (1st+2nd) piezoelectric potential within the region of interest. The fact that the 1st order and the 2nd order terms oppose each other is also noticeable in *Figure 4.6*, which depicts the surface plots of the piezoelectric potential distribution in the *XY* plane. Note that the 1st order term has got somewhat larger magnitude and spread than the quadratic term. Also, associated with both these two terms, noticeable is the asymmetry and non-equivalence (in terms of potential magnitude and distribution) along the [110] and the [1$\underline{1}$0] directions.
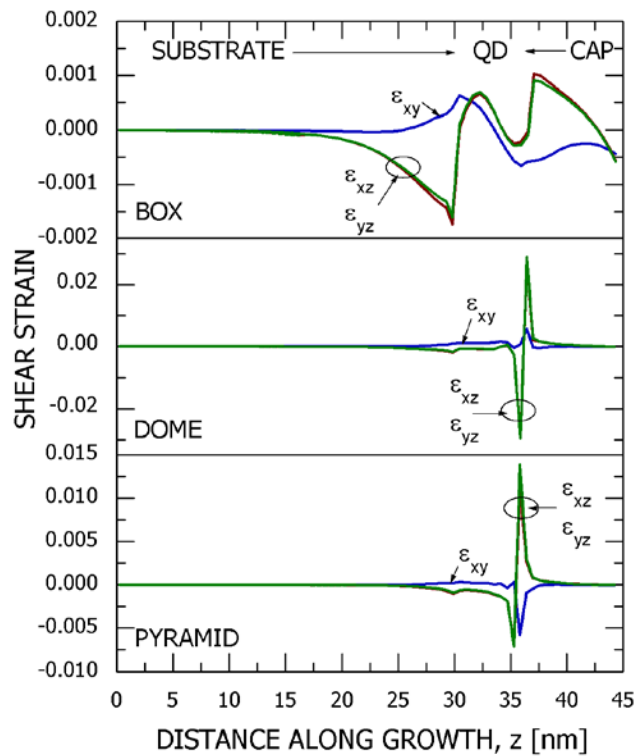
Figure 4.4 Atomistic shear strain profiles along the *z* (growth) direction that, in effect, induces polarization in the sample. Note the varying spread/penetration in the surrounding material matrix as a function of dot shape.
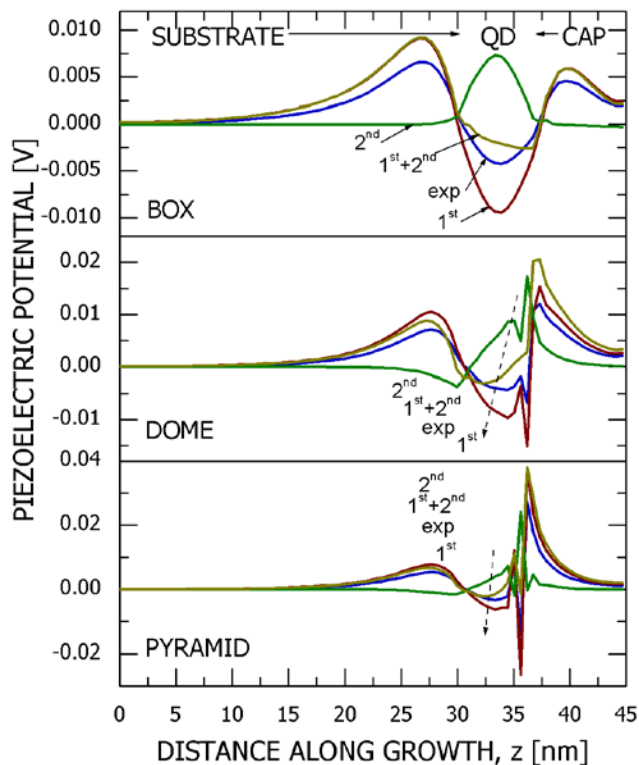
Figure 4.5 Induced piezoelectric potential along the *z* (growth) direction in all three quantum dots. Four different models for the polarization constants have been used in the calculations[18], (1) linear and experimentally measured, (2) linear through *ab initio* calculations, (3) quadratic through *ab initio* calculations, and (4) combination of 1st and 2nd order components. The varying spread/penetration of the potential in the surrounding material matrix as a function of dot shape is shown in the figure.
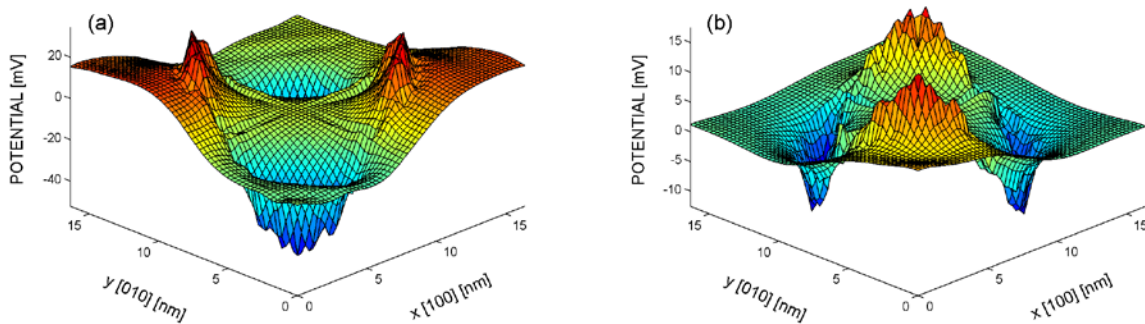
.

Figure 4.6 Linear and quadratic contributions of the piezoelectric potential in the *XY* plane halfway through the dot height. Note the magnitude, orientation, and anisotropy in the induced potential.

Figure 4.7 shows the first 4 (four) conduction band wavefunctions for all three quantum dots including *both* the strain and the piezoelectric fields (4th model) in the calculations. The piezoelectric potential introduces a global shift in the energy spectrum and generally opposes the strain induced field. In box and dome shaped dots, the net piezoelectric potential is found to be strong enough to fully offset the combined effects of interface and strain fields and, thereby, *flip* the optical polarization anisotropy. Also shown in *Figure 7* are the splits in the P levels (ΔP) for all three quantum dots. To get a overview about various factors affecting the piezoelectric potential we have prepared Table 4.I that quantifies the *individual* net contributions from crystal atomicity and interfaces, strain, and the various components of piezoelectric fields in the spilt of the P level. The net piezoelectric contribution is found to be largest in a box and minimum in a pyramid, which clearly establishes a one-to-one correspondence between the piezoelectric potential and the volume of the quantum dot under study.

BOX: $E_{1\bar{1}0} - E_{110} = -8.0$ meV

DOME: $E_{1\bar{1}0} - E_{110} = -4.0$ meV

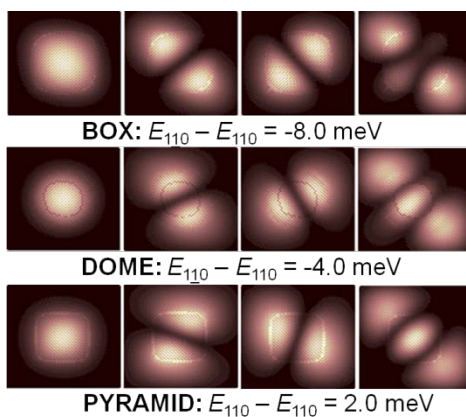PYRAMID: $E_{1\bar{1}0} - E_{110} = 2.0$ meV

Figure 4.7 First 4 (four) electronic wavefunctions and split in the P levels in all three quantum dots including atomicity/interfacial effects, strain, and piezoelectricity. Note the varying piezoelectric contributions, which can be attributed mainly to the volume of the quantum dot under study.

Table 4.1 Peizoelectric Potential caused due to various effects in BOX, DOME and PYRAMID Quantum Dots.

Effect	BOX (meV)	DOME (meV)	PYRAMID (meV)
Atomicity Interface	1.2	-7.4	3.56
Strain Relaxation	1.4	13.3	3.24
Interface + Strain	2.6	5.9	6.8
PZ (1st Order)	-12.6	-16.9	-10.8
PZ (2nd Order)	0.4	5.1	5.2
PZ (1st + 2nd Order)	-10.6	-9.9	-4.8

1st + 2nd →1.357
2nd →1.354
1st →1.357
Exp →1.357

1st + 2nd →1.343
2nd →1.346
1st →1.344
Exp →1.343

1st + 2nd →1.328
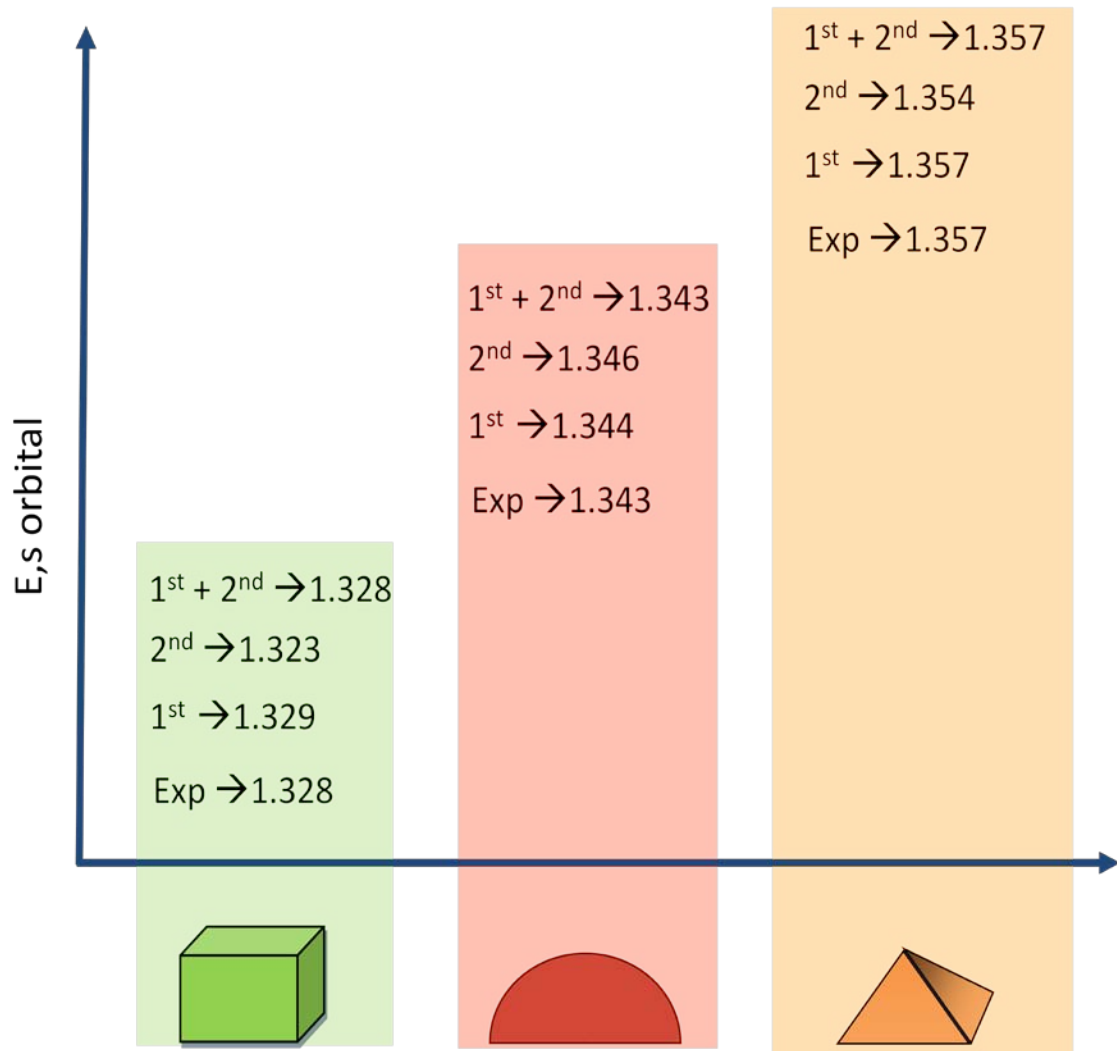2nd →1.323
1st →1.329
Exp →1.328

E,s orbital

Figure 4.8 graphically represents the geometric dependence of shape of Quantum Dots affecting the shift in 1-particle energy states.

4.2 SIMULATION RESULTS FOR QUANTUM WELL STRUCTURE (HEMT):

Figure 4.9 shows the channel region of HEMT Heterostructure. The structure considered in this work is made up AlN/GaN materials. From bottom we have GaN substrate layer 30nm thick, above that we have InN wetting layer of 1nm thickness. Over that we have the undoped channel region made of GaN layer which is 25nm thick and finally we have a highly doped AlN region of 13nm

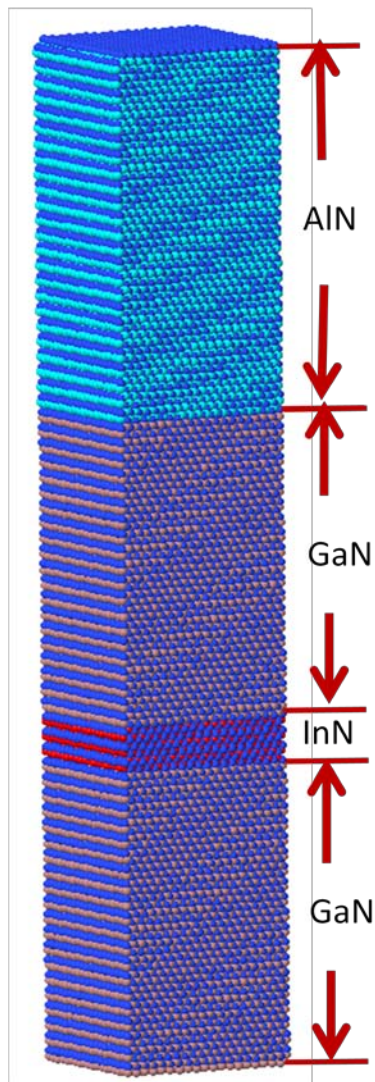thickness. This figure illustrates the atomic representation of channel region of HEMT.

Figure 4.9 Structure of materials in HEMT channel region

Figure 4.10 shows the Peizo and pyro electric potential contour, where we

see there exist a net dipole moment due in piezoelectric potential due to effect of built in fields. It also shows the high pyroelectricity of around 70mV. Figure 4.10 shows the comparison of both Piezo and pyro electric potentials. Many research groups are working to engineer this huge pyroelectric potential to reduce heat in the HEMT structure.
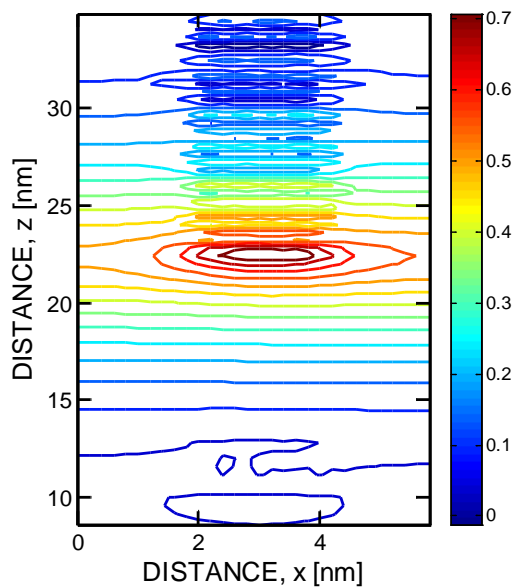
PIEZOELECTRIC
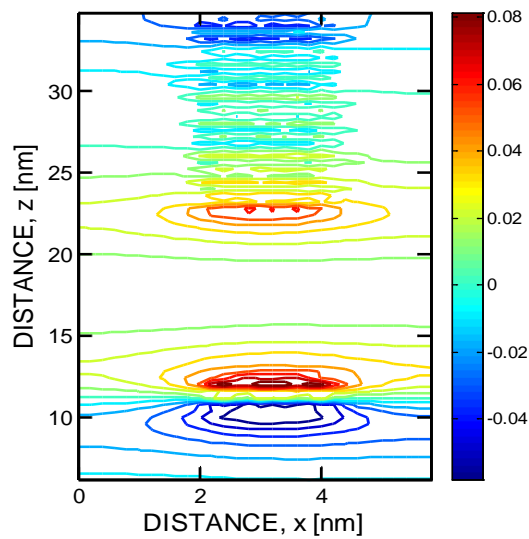
PYROELECTRIC

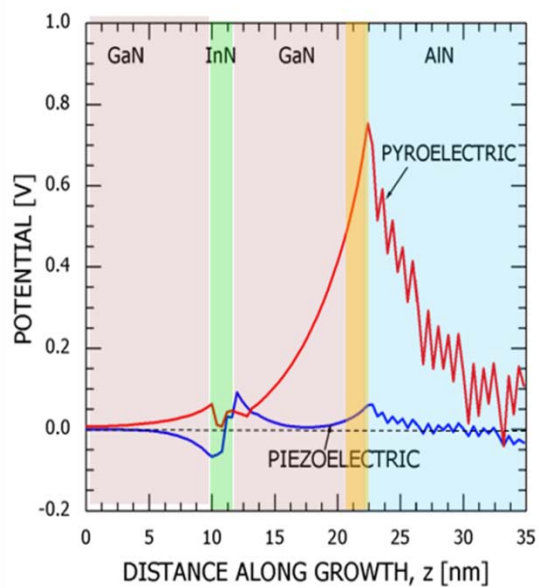Figure 4.10 Piezo and Pyro potential contour

Figure 4.11 Comparison of Piezo and Pyro electric potential profile

4.3 Conclusion:

Atomistic simulations using the NEMO 3-D tool have been performed to study the origin, nature and the effect of the built-in electrostatic fields in Zincblende InAs/GaAs quantum dots with 3 (three) different shapes, namely, box, dome, and pyramid, all having a diameter/base length of 11.3 nm and a height of 5.6 nm and Wurtzite AlN/GaN HEMT. The atomistic strain fields (both hydrostatic and shear) are long-ranged and penetrate deep into the substrate and cap layer. Box Quantum Dot has the largest spread (~15nm) inside the surrounding material. As opposed to the atomic/interfacial symmetry, strain is found to have a general/uniform tendency to orient the electronic wave functions along the [110] direction and further lower the symmetry of the system under study. Dome Quantum Dot is found to have the highest strain field. Regarding piezoelectricity, for the first time, 4 (four) different models for polarization have been implemented within the atomistic tight-binding description. In contrast with the findings of Ref. [20], we find that, *within* the quantum dot region, the contributions from the linear and the quadratic terms have comparable magnitudes, even though they are oppose each other, the linear term is is very large when compared to that of quadratic term. Hence there exists a non vanishing net piezoelectric potential. The quadratic term, therefore, cannot be neglected and must be taken into account. This particular observation essentially stresses the need for using *realistically-extended* substrate and cap layers (simulation domains containing ~2 million atoms) in the numerical modeling of these reduced-dimensional quantum dots. We also recommend that the high

pyro-electric potential observed in the HEMT can be engineered to reduce the

heating in the device.

REFERENCES

[1]   Shaikh Shahid Ahmed, "Modelling Quantum and Coulomb effects in Nanoscale Devices*", Dissertation for phD,* May 2005.

[2]   B. Van Zeghbroeck, "Principles of Semiconductor Devices*",* 2007.

[3]   Wikipedia - *http://en.wikipedia.org/wiki/MOSFET*.

[4]   Tosh*iba - http://www.toshiba-components.com/ASIC/Technology.html*

[5]   HS Wong, "Beyond the conventional transistor," *IBM J., Res. & Dev.* vol.   46 pp. 133–168, march/may 2002.

[6]   W. Zhu, J. P. Han, T. P. Ma, Mobility Measureme*nt and Degradation* Mechanisms of MOSFETs Made With Ultrathin High-k Dielectrics, *IEEE Trans. Electron Dev.*, vol. 51, pp. 98–105, 2004.

[7]   Welser, J. L. Hoyt and J. F. Gibbons, "NMOS and *PMOS transistors fabrica*ted in strained silicon/relaxed silicon-germanium struct*ures," IEDM Tech. Dig.,* 1000–1002, 1992.

[8]   G. Formicone, D. Vasileska, D.K. Ferry, "2D Monte Carlo simulation of hole and electron transport in strained Si," *VLSI Design*, vol. 6, *pp. 167–171, 1998.*

[9]   D. *V*asileska, G. Formicone and D.K. Ferry, "Doping dependence of the mobility enhancement in surface-channel strain*ed-Si layer*s,*" Nanotechnology*, vol. 10, pp. 147–152, 1999.

[10]   R. Oberhuber, G. Zandler, and P. Vogl, "Subband structure and mobility of two–dimensional holes in strained S*i/SiGe MOSFET'*s," *Phys. Rev. B, vo*l. 58, pp. 9941–9948, 1998.

[11]   P. M. Garone, V. Venkataraman, and J. C. Sturm, "Hole mobility enhancement in MOS-gated Ge_xSi_{1-x}/Si heterostructure inversion layers," *IEEE Electron Device Lett.*, vol. 13, pp. 56–58, 1992.

[12]   Herbert Kroemer, "Heterostructure Bipolar Transistors and Integrated Circuits," *IEEE*, vol. 70, NO. 1, January 1982.

[13]   Shaikh Shahid Ahmed, "Modelling of Silicon On Insulator Devices,*" Thesis for Master of Science degree,* May 2003.

[14]   B.R. Nag, "Physics of Quantum Well Devices," 2000.

[15]   Fabio Alessio Marino, Nicolas Faralli, Tomas Palacios, David K. Ferry, Stephen M. Goodnick and Marco Saraniti, "Effects of Threading Dislocations

on AlGaN/GaN High-Electron Mobility Transistors," *IEEE transactions on Electron Devices,* vol. 57,No. 1, January 2010.

[16]   GaN RF Market 2008 Report, *www.mindbranch.com/ GaN-RF-R393-82/*

[17]   U.K. Mishra, P. Parikh and Y.F. Wu, "AlGaN/GaN HEMTs: An overview of device operation and applications," *IEEE,* vol.90, No. 6, June 2002.

[18]   Saburo Takamiya, Naohito Yoshida, Norio Hayafuji, takuji Sonoda and Shigeru Mitsui, "Overview of Recent development of HEMTs in the mm-Wave Range," *Solid-State Electronics,* vol. 38, No. 9, pp. 1581-1588, 1995.

[19]   Wikipedia - *http://en.wikipedia.org/wiki/High_Electron_Mobility_Transistor*

[20]   Travis J. Anderson, Marko J. Tadjer, Michael A. Mastro, Jennifer K. Hite, Karl D. Hobart, Charles R. Eddy, Jr., and Francis J. Kub, "An Ultrathin AlGaN/GaN HEMT Structure for Enhancement Mode Operation using Selective Etching," *IEEE Electron Device Letters*, vol. 30, No. 12, December 2009.

[21]   C.Y.Chang, S.J. Pearton, C.F. Lo, F.Ren, I.I.Kravchenko, A.M. Dabiran, A.M. Wowchak, B. Cui and P.P.Chow, "Development of Enhancement Mode AlN/GaN High Electron Mobility Transistors," *Applied Physics Letters*, 94, 263505 (2009).

[22]   Sammy Kayali, George Ponchak, Roland Shaw, "GaAs MMIC Reliability Assurance Guidelines for Space Applications," *Jet Propulsion Laboratory,* 96-25, 1996.

[23]   Lingjia Li, Marek Skowronski, "Gate I-V Characteristic Degradation in AlGaN/AlN/GaN HEMT," *ISDRS ,College Park MD, USA ,* 2007.

[24]   Roberto Menozzi, "Tropical Review – Hot electron effects and degradation of GaAs and InP HEMTs for microwave and millimeter-wave applications," *Semicond. Sci. Technol.* 13 (1998) 1053-1063.

[25]   Yu-Suyan Lin, Yi-Wei Lain and Shawn S.H. Hsu, "AlGaN/ GaN HEMT's with Low Leakage Current and High On/Off Current Ratios," *IEEE Electron Device Letters,* vol. 31, No. 2, February 2010.

[26]   Fabio Sacconi, Michael Povoloskyi, Aldo Di Carlo, "Strain Defects in SiN passivated GaN based HEMT devices," *J Comput Electron* (2006) 5: 115 - 118.

[27]   B. S. Kang, S. Kim, J. Kim, F. Ren, K. Baik, S. J. Pearton, B. P. Gila, C. R. Abernathy, C.-C. Pan, G.-T. Chen, J.-I. Chyi, V. Chandrasekaran, M. Sheplak, T. Nishida and S. N. G. Chu, "Effect of strain on the conductivity of

AlGaN/GaN high-electron-mobility transistors," *Appl. Phys. Lett.*, Vol. 83, No. 23, 8 December 2003.

[28] Nadeemullah A. Mahadik, Syed B. Qadri, and Mulpuri V. Rao, *Appl. Phys. Lett.* 93, 222106 (2008).

[29] Jasprit Singh, "PHYSICS OF SEMICONDUCTORS AND THEIR HETEROSTRUCTURES," *ISBN 0-07-057607-6*, 1993.

[30] Ambacher, O., Foutz, B., "Two dimensional electron gases induced by spontaneous and piezoelectric polarization in undoped and doped AlGaN/GaN heterostructures," *Journal of Applied Physics*, 00218979, Vol. 87, Issue 1, 01/01/2000.

[31] W. Q. Chen and S. K. Hark, *J. Appl. Phys.* 77, 5747 (1995).

[32] A.Bykhovski, B. L. Gelmont, and M. S. Shur, *J. Appl. Phys.* 81, 6332 (1997).

[33] O. Ambacher, J. Smart, J. R. Shealy, N. G. Weimann, K. Chu, M. Murphy, W. J. Schaff, L. F. Eastman, R. Dimitrov, L. Wittmer, M. Stutzmann, W. Rieger, and J. Hilsenbeck, *J. Appl. Phys.* 85, 3222 (1999).

[34] F. Bernardini, V. Fiorentini, and D. Vanderbilt, *Phys. Rev.* B 56, R10024 (1997).

[35] G. D. O'Clock and M. T. Duffy, *Appl. Phys. Lett.* 23, 55 (1973).

[36] K. Tsubouchi, K. Sugai, and N. Mikoshiba, *IEEE Ultrason. Symp.* 1, 375 (1981).

[37] K. Shimada, T. Sota, and K. Sizuki, *J. Appl. Phys.* 84, 4951 (1998).

[38] S. Barker, Jr. and M. Ilegems, *Phys. Rev.* B 7, 743 (1973).

[39] SHAIKH AHMED, NEERAV KHARCHE , RAJIB RAHMAN, MUHAMMAD USMAN, SUNHEE LEE, HOON RYU, HANSANG BAE, STEVE CLARK, BENJAMIN HALEY, MAXIM NAUMOV, FAISAL SAIED, MAREK KORKUSINSK, RICK KENNEL, MICHAEL MCLENNAN, TIMOTHY B. BOYKIN, AND GERHARD KLIMECK, "Multimillion Atom Simulations with NEMO 3-D".

[40] Gerhard Klimeck, "Nano Electronic MOdelling: NEMO", Network of Computational Nanotechnology (NCN), http://nanohub.org/resources/3707.

[41] Dragica Vasileska, "Introduction to Silvaco TCAD ATLAS", Computational Electronics presentation, http://nanohub.org/resources/1517.

[42] www.silvaco.com

[43]   F. Bernardini, V. Fiorentini and D. Vanderbilit, *Phy Rev,* B 56, R 10024 (1997).

[44]   K. Tsubouchi, K. Sugai and N. Mikoshiba, *IEEE Ultrason. Symp,*1, 375 (1981).

[45]   G. D. O'Clock and M. T. Duffy, *App.l Phys. Lett,* 23, 55 (1973).

[46]   M. A. Littlejohn, A. R. Hauser and T. H. Glisson, *App.l Phys. Lett,* 26, 625, (1975).

[47]   K. Shimada, T. Sota and K. Sizuki, *J. Appl. Phys,* 84, 4951 (1998)

[48]   K. Shimada, T. Sota, K. Sizuki and H. Okumura, *J. Appl. Phys,* part 2 37, L 1423 (1998).

[49]   S. barker, Jr. and M. Ilegems, *Phys. Rev,* B 7, 743 (1973).

[50]   F. Bernardini and V. Fiorentini, *Phys. Rev,* B 79, 3958 (1997).

[51]   Bimberg, Marius Grundmann, Nikolai N. Ledentsov, "Quantum Dot Heterostructures ," 1999, ISBN 0-471-97388.

[52]   Sharnali Islam, Sasi Sundaresan, and Shaikh Ahmed, "Geometry Dependence of the Internal Fields and Its Impact on the Electronic Structure in Self-Assembled InAs/GaAs Quantum Dots", *Submitted to IEEE Trans on NanoTechnology,* OCT 2009.

[53]   Bcc research - http://www.bccresearch.com/report/NAN027B.html

[54]   Wiki - http://en.wikipedia.org/wiki/Quantum_dot#Colloidal_synthesis

[55]   Evident Technologies - http://www.evidenttech.com/quantum-dots-explained/how-quantum-dots-work.html

[56]   Wiki - http://en.wikipedia.org/wiki/Quantum_dot_laser

VITA

Graduate School
Southern Illinois University

Sasi S. Sundaresan   Date of Birth: May 10, 1987

800 E Grand Ave Apt#38B, Carbondale, Illinois 62901

Email: hexas_sas@yahoo.com

Anna University, Chennai
Bachelor of Engineering, Electronics & Instrumentation, May 2008

Thesis Title:
    Effects of Internal Fields in Quantum Dots

Major Professor: Shaikh S. Ahmed

Publications:
    Sharnali Islam, Sasi Sundaresan, and Shaikh Ahmed, "Geometry Dependence of the Internal Fields and Its Impact on the Electronic Structure in Self-Assembled InAs/GaAs Quantum Dots", *Submitted to IEEE Trans on NanoTechnology,* OCT 2009.